Pharmacoinformatics-based prediction of potential Keap1 inhibitors from Hemidesmus indicus (L) R.Br. against oxidative stress-induced diseases

Senthilkumar Vellur
Kalasalingam Academy of Research and Education
Parasurman Pavadai
M.S. Ramaiah University of Applied Sciences, M S R Nagar
Chandrasekar Palanichamy
Kalasalingam Academy of Research and Education
Shanmugampillai Jeyaraguru Kabilan
Kalasalingam Academy of Research and Education
Sureshbabu Ram Kumar Pandian
Kalasalingam Academy of Research and Education
Selvaraj Kunjiappan (selvaraj.k@klu.ac.in)
Kalasalingam Academy of Research and Education

Research Article

Keywords: Oxidative stress, Hemidesmus indicus (L) R.Br., Keap1-Nrf2, molecular docking, antioxidant

Posted Date: November 14th, 2022

DOI: https://doi.org/10.21203/rs.3.rs-2255631/v1

Abstract

The Keap1-Nrf2 pathway plays a prominent role in activating cytoprotective genes, detoxification and antioxidative defense enzymes against oxidative stress and xenobiotics-induced damage. Oxidative stress is involved in the initiation and progression of numerous health complications. The present study investigated the antioxidant potential of aqueous methanolic extract of *Hemidesmus indicus* (L) R.Br., followed by a pharmacoinformatics-based screening of novel Keap1 protein inhibitors. Initially, the antioxidant potential of this target plant was assessed by antioxidant assays (DPPH, ABTS radical scavenging and FRAP). H. indicus (L) R.Br. extract (100 µg mL^{-1}) showed 85 ± 2.917%, 78.783 ± 0.24% of DPPH, ABTS radicals scavenging activity, and 161 ± 4 µg mol (Fe (II)) g^{-1} ferric ion reducing power. Further, a total of sixty-nine phytocompounds were derived from this plant through the IMPPAT database, and their three-dimensional structures were obtained from the PubChem database. The chosen sixty-nine phytocompounds were docked against the Kelch-Neh2 complex protein (PDB entry ID: 2flu, resolution 1.50 Å) along with the standard drug (CPU192018). The top scored three hits were selected, namely Hemidescine (– 11.30 Kcal mol^{-1}), Beta-Amyrin (– 10.00 Kcal mol^{-1}), and Quercetin (– 9.80 Kcal mol^{-1}) based on their binding affinities. The selected three hits showed significant drug-likeness properties with the least toxicity profile. Molecular dynamics simulation studies showed that all the protein-ligand complexes (Keap1-HEM, Keap1-BET and Keap1-QUE) were highly stable during the entire simulation period, compared to standard CPUY192018-Keap1complex. Based on these findings, the top-scored three phytocompounds may be used as a significant and safe Keap1 inhibitor and could potentially use for oxidative stress-induced health complications.

Introduction

Oxygen is an essential element in the respiratory processes of most living cells (1). When cells utilize oxygen by breakdown of biomolecules to generate energy in the form of ATP (adenosine triphosphate), and free radicals as an unavoidable by-product in mitochondria (2). Generally, the produced free radicals are highly reactive atoms with one or more unpaired electrons in their external shell. Free radicals can quickly loss or gain a single electron, acting as powerful oxidants or reductants (3). These free radicals are generally termed as reactive oxygen species (ROS), reactive-nitrogen species (RNS) and DNA reactive aldehyde (DRA) (4). ROS is a double-edged sword with functional (lower level) and harmful effects (higher level) (5). At lower level, ROS is essential for protein phosphorylation, transcription factor activation, cell cycle, cell division, cellular proliferation, migration, and programmed cell death, as well as some metabolic functions; while higher level of ROS causes oxidative damage and leads to irreparable damage of the cell (6). Accumulative evidence indicates that oxidative stress has been linked to numerous pathological consequences, including cancer, diabetes mellitus, cardiovascular diseases, inflammation, ageing and neurodegenerative diseases (Alzheimer's, epilepsy, and Parkinson's)(7, 8).

In order to maintain the level of ROS in cells by scavenging free radicals through several enzymatic and non-enzymatic antioxidant cellular defense mechanisms (9). The detoxifying enzymes and non-enzymatic antioxidants play a significant role in protecting cells, organs and tissues from toxins and oxidative stress (10). Oxidative stress responsive genes sensitize to secreting primary antioxidant enzymes against free radicals includes, superoxide dismutase (SOD), catalase (CAT), glutathione peroxidase (GPx), peroxiredoxins (11). Conversely, non-enzymatic antioxidants (carotenoids, vitamins A, C and E, flavonoids, alpha-lipoic acid glutathione) interrupt free radical chain reactions (12). In addition, the elevated intracellular ROS levels above a certain threshold result in the downregulation of cellular antioxidant pathways and enzyme systems, which leads to the development of numerous complications via a variety of molecular targets, including nuclear factor-B (NF-B), nuclear factor E2 (erythroid-derived 2)-related factor 2 (Nrf2), Kelch-like ECH-associated protein 1 (Keap1), mitogen-activated protein kinases (MAPKs), and phosphoinositide 3-kinase (PI3K)(13–15).

The Nrf2 is a potential transcriptional activator that coordinates basal and stress-inducible activation of numerous cytoprotective genes against oxidative stress (16). Target genes of Nrf2 are involved in drug transport, xenobiotic metabolism, glutathione production, and ROS removal (17). Keap1 is a cytoplasmic protein, and it is a predominant negative regulator of Nrf2 (18). In a Keap1-dependent manner, Nrf2 is continuously destroyed under basal conditions by the ubiquitin-proteasome pathway (19). By preventing the ubiquitin-proteasome system from degrading Nrf2, inhibition of Keap1 activity can accumulate newly synthesized Nrf2 and cause it to move to the nucleus, where it triggers the transcription of several antioxidative and cytoprotective genes, ultimately activating the cell defense system (20).

Plenty of research work indicates that plant-derived phytocompounds that confer effective free-radical scavenging activities that may, in turn, reduce the ROS-induced oxidative stress and enhance antioxidative defense mechanisms (21). In addition, plant-derived antioxidants more preferable to synthetic ones because synthetic antioxidants have negative health consequences when used for more extended periods of time (22). In recent years, there has been a lot of interest in Indian traditional medicinal systems and the use of plant-derived drugs as an alternative option to treat various complications including cancer, diabetes, cardiovascular, neurodegenerative diseases, etc.,(23). Hemidesmus indicus (L) R.Br. belonging to the Asclepiadaceae family often known as “Indian Sarsaparilla”, is a twining shrub that has been used as a folk medicine and as an ingredient in Siddha, Ayurvedic and Unani medicines against inflammation, blood, and other ailments (24). Several studies have established that the phytochemical profile of the root of H. indicus (L) R.Br. extract has 2-hydroxy-4-methoxy-

benzoic acid, b-sitosterol, α- and β-amyrins, nerolidol, caryophyllene, borneol, lupeol, tetracyclic triterpene alcohols, hemidesminin, hemidesmin-1 and 2, resin acids, fatty acids, tannins, glycosides and a ketone, etc., which are being used for the treatment of several complications (25). Hence, the present study was designed to evaluate in vitro free-radical quenching potential of a crude extract of H. indicus (L) R.Br. Further, the study was extended to predict potential Keap1 inhibitors from target plant H. indicus (L) R.Br. to neutralize the excessive ROS generation through in silico molecular docking and dynamics simulation tools. In addition, the pharmacokinetic and physicochemical properties of the screened phytocompounds were also studied.

Results

Antioxidant power

DPPH radical scavenging assay

Figure 1(a) shows the free radical scavenging effect of varying concentrations of *H. indicus* (L) R.Br. extract on DPPH radical. The observed results shows that varied concentrations of 100, 75, 50, 25, 12.5, and 6.25 µg mL^{-1} *H. indicus* (L) R.Br. extract displayed 85 ± 2.917%, 67.667 ± 1.416%, 42.643 ± 1.335%, 34.897 ± 1.096%, and 24.523 ± 2.159% respectively, in a concentration-based manner. Further, 6.25 µg mL^{-1} of rutin showed 34.72 ± 3.999% scavenging of DPPH radicals.

Abts Radical Scavenging Assay

The standard drug has been used to compare the relative antioxidant effects to scavenge the ABTS radical. Using potassium persulphate, the stable form of the ABTS radical cation was generated. After producing stable absorbance, the reaction medium is supplemented with an antioxidant *H. indicus* (L) R.Br. extract, and the antioxidant power is measured by observing decolorization. The varied concentrations of 100, 75, 50, 25, 12.5, and 6.25 µg mL^{-1} of *Hemidesmus indicus* extract scavenged ABTS radical in a concentration-dependent mode as shown in Fig. 1(b). At a maximum concentration (100 µg mL^{-1}) of aqueous methanolic extract of *H. indicus* (L) R.Br. exhibited highest (78.783 ± 0.24%) decolourization of ABTS radicals.

Frap Assay

When an *H. indicus* (L) R.Br. extract (antioxidant) reacts with a ferric tripyridyltriazine (Fe^{3+} -TPTZ) complex to produce a coloured ferrous tripyridyltriazine (Fe^{2+} -TPTZ), the FRAP assay determines the reducing potential of the ferric ions. The free radical chain breaking takes place by donating an electron. Varied concentrations of aqueous methanolic extract of *H. indicus* (L) R.Br. extracts were screened by FRAP assay along with standard ascorbic acid. In the results obtained, the better reducing potential was exhibited 161 ± 40 µg mol^{-1} (Fe(II)) g^{-1} at a concentration of 100 µg mL^{-1} of *H. indicus* (L) R.Br. extract. In the observed results, *H. indicus* (L) R.Br. extract showed higher activity than reference standard ascorbic acid as shown in Fig. 1(c).

Active Compounds Library

The identified sixty-nine active compounds from *H. indicus* (L) R.Br. along with standard drug CPUY192018 and their 3-dimensional structures were listed in Table 1. Selected compound structures were optimized and used *in silico*molecular docking against chosen protein, Kelch-Neh2 complex.

Table 1
Phytocompounds found in *Hemidesmus indicus* (L) R.Br. and their binding affinity against Keap1

S. No	Compound id (CID)	Active compound	Docking score (Kcal.mol^{-1})
1.	379	Octanoic acid	-4.6
2.	643731	trans-2,cis-6-Nonadienal	-4.7
3.	2969	Decanoic acid	-4.8
4.	785	Hydroquinone	-5.0
5.	12412	Hexatriacontane	-5.0
6.	21146488	(1S,3aR,5aR,5bR,7aS,11aS,11bR,13aR,13bR)-3a,5a,5b,8,8,11a-hexamethyl-1-propan-2-yl-1,2,3,4,5,6,7,7a,9,10,11,11b,12,13,13a,13b-hexadecahydrocyclopenta[a]chrysene	-5.0
7.	460	Guaiacol	-5.1
8.	6998	Salicylaldehyde	-5.1
9.	31244	4-Methoxybenzaldehyde	-5.1
10.	3893	Lauric acid	-5.2
11.	22311	Limonene	-5.2
12.	9007	3-Methoxyphenol	-5.3
13.	985	Palmitic acid	-5.6
14.	2758	Eucalyptol	-5.7
15.	4133	Methyl salicylate	-5.7
16.	69600	2-Hydroxy-4-methoxybenzaldehyde	-5.7
17.	1183	Vanillin	-5.7
18.	444539	Cinnamic acid	-5.8
19.	8294	Linalyl acetate	-5.8
20.	12127	Isovanillin	-5.9
21.	11230	4-Carvomenthenol	-5.9
22.	61130	Myrtenal	-5.9
23.	29025	Verbenone	-5.9
24.	93046	2,10-Epoxypinane	-5.9
25.	6552009	d-Borneol	-6.0
26.	10582	Myrtenol	-6.0
27.	6989	Thymol	-6.0
28.	17100	alpha-Terpineol	-6.0
29.	121719	Pinocarvone	-6.1
30.	5355854	Pentyl cinnamate	-6.2
31.	5284507	Nerolidol	-6.2
32.	5281522	Isocaryophyllene	-6.3
33.	2537	Camphor	-6.3
34.	3469	2,5-Dihydroxybenzoic acid	-6.4

S. No	Compound id (CID)	Active compound	Docking score (Kcal.mol^{-1})
35.	6448	Bornyl acetate	-6.4
36.	30248	Dihydrocarvyl acetate	-6.4
37.	75231	4-Methoxysalicylic acid	-6.4
38.	8468	Vanillic acid	-6.4
39.	637542	4-Hydroxycinnamic acid	-6.5
40.	6918391	beta-Elemene	-6.6
41.	6950273	Isobornyl acetate	-6.6
42.	72	3,4-Dihydroxybenzoic acid	-6.6
43.	10742	Syringic acid	-6.6
44.	3102	Benzophenone	-6.7
45.	370	Gallic acid	-6.8
46.	111037	alpha-Terpinyl acetate	-6.8
47.	689043	Caffeic acid	-6.8
48.	445858	Ferulic acid	-6.9
49.	91354	Aromadendrene	-6.9
50.	92812	Ledol	-7.0
51.	5369459	Phenethyl cinnamate	-7.1
52.	2345	Benzyl benzoate	-7.1
53.	442343	Levomenol	-7.3
54.	100949538	alpha-Muurolol	-7.5
55.	442393	beta-Selinene	-7.5
56.	5280804	Isoquercitrin	-8.8
57.	5281643	Hyperoside	-8.8
58.	9548870	Ursane	-8.9
59.	92157	Lupeol acetate	-9.0
60.	5280805	Rutin	-9.1
61.	259846	Lupeol	-9.1
62.	222284	beta-Sitosterol	-9.3
63.	9548717	Oleanane	-9.5
64.	92156	beta-Amyrin acetate	-9.6
65.	16129778	Tannic acid	-9.6
66.	73170	alpha-Amyrin	-9.7
67.	5280343	Quercetin	-9.8
68.	73145	beta-Amyrin	-10
69.	101664025	Hemidescine	-11.3

S. No	Compound id (CID)	Active compound	Docking score (Kcal.mol^{-1})
Standard Drug			
70.	73330369	CPUY192018	-9.10

Active Binding Site Identification

The predicted active binding sites of the target protein (Kelch-Neh2 complex) are presented in Fig. 2. The Prank Web tool revealed that there are three important binding sites where the active ligands interact and trigger conformational changes. The predicted binding pockets were presented in three different colors (blue, red, and green). The first binding pocket (blue colour) is the highest score of all three pockets, with a pocket score of 5.91, 18 amino acids, and a probability score was 0.310. The second binding pocket (red colour) with a pocket score of 4.11, 14 amino acids, and a probability score was 0.176. And, the third binding pocket (green colour) had the least pocket score of 1.21, 8 amino acids, and a probability score was 0.012. The structure-based molecular screening of the selected phytocompounds were evaluated using the same identified binding pockets of the keap1 protein. In the molecular docking studies, receptor grid construction resulted in more reliable ligand posture scoring. As a result, based on the previously acquired binding site residues, we constructed a receptor grid for the selected Kelch-Neh2 complex protein in order to obtain a more exact scoring of our ligand-binding poses. The receptor grid with a box dimension of X = 64.30 Å, Y = 53.75 Å, and Z = 48.41 Å was created and used for molecular docking analysis.

Molecular Docking

The intermolecular interaction between the target protein and active compounds was investigated using in silico molecular docking method. Using the PyRx tool in the AutoDock Vina program, a certain number of bioactive compounds (sixty-nine) and a standard drug CPUY192018 were docked against Kelch-Neh2 complex protein to analyze their binding potential. Ten bioactive compounds were shown to have a significant binding affinity (> − 09.00 kcal mol^{-1}) against the target Kelch-Neh2 complex protein. Following molecular docking investigations, it was discovered that the bioactive compounds' binding energies were dispersed, ranging from − 4.60 to -11.30 Kcal mol-1, as shown in Fig. 3 and Table 2. The top three compounds (Hemidescine (− 11.30 Kcal mol^{-1}), Beta-Amyrin (− 10.00 Kcal mol^{-1}), and Quercetin (− 9.80 Kcal mol^{-1})) were chosen for future research based on their binding energy with the amino acid residues in the active site of Kelch-Neh2 complex protein. Along with this study, we used a standard drug CPUY192018 (− 9.10 Kcal mol^{-1}).

Table 2
Pharmacokinetics and physicochemical parameters of selected bioactive compounds and standard drug CPUY192018.

Parameter	Hemidescine (CID: 101664025)	Beta-Amyrin (CID: 73145)	Quercetin (CID: 5280343)	CPUY192018 (CID: 73330369)
Formula	$C_{36}H_{58}O_{10}$	$C_{30}H_{50}O$	$C_{15}H_{10}O_7$	$C_{28}H_{26}N_2O_{10}S_2$
MW ($g.mol^{-1}$)	650.84	426.72	302.24	614.64
Num. heavy atoms	46	0	22	42
Num. arom. heavy atoms	0	12	16	22
Fraction Csp3	0.92	0.93	0.00	0.14
Num. rotatable bonds	8	0	1	12
Num. H-bond acceptors	10	1	7	10
Num. H-bond donors	3	1	5	02
Molar Refractivity	171.72	134.88	78.04	154.12
TPSA (Å²)	131.14	20.23	131.36	184.58
Solubility class	Moderately soluble	Poorly Soluble	Soluble	Moderately soluble
GI absorption	Low	Low	High	Low
BBB permeation	No	No	No	No
Violation of Lipinski's rule of five	1	1	0	2
Violation of Veber rule	Yes	Yes	Yes	2
Bioavailability Score	0.55	0.55	0.55	0.11
Synthetic accessibility	8.01	6.04	3.23	3.83

Interpretation Of Receptor–ligand Interactions

Hemidescine (HEM) created three hydrophobic contacts ALA366X (3.77 Å), VAL514X (3.65 Å), VAL561X (3.80 Å), while GLY367X (2.89 Å), ARG415X (2.67 Å), ILE416X (2.32 Å), VAL418X (2.76 Å), VAL561X (3.26 Å), VAL561X (2.68 Å), GLN563X (3.33 Å) formed seven hydrogen bonds and one salt bridge ARG326X (4.85 Å) with the target protein, as presented in Fig. 3(a) and 3(b). Beta-Amyrin (BET) formed four hydrophobic interactions with ALA336X (3.90 Å), VAL418X (3.44 Å), VAL514X (3.51 Å), VAL561X (3.93 Å) target protein, as depicted 4c and 4d. Quercetin (QUE) contacted with one hydrophobic bonding ALA366X (3.93 Å), and eight hydrogen bonding GLY367X (2.14 Å), ARG415X (1.89 Å), ARG415X (2.30 Å), VAL465X (2.31 Å), VAL465X (2.44 Å), ALA510X (2.08 Å), VAL512X (2.72 Å), VAL606X (2.39 Å) with the target protein, as depicted in Fig. 4e and 4f. Standard drug CPUY192018 (CPU) formed three hydrophobic bonding ALA366X (3.96 Å), VAL418X (3.22 Å), ILE559X (3.71 Å), and nine hydrogen bonding ARG326X (2.91 Å), GLY367X (2.89 Å), VAL418X (1.80 Å), VAL465X (2.58 Å), VAL467X (2.06 Å), ILE559X (2.05 Å), VAL561X (2.41 Å), VAL606X (2.28 Å), VAL606X (3.37 Å) with the target protein, as depicted in 4g and 4h.

In silico **prediction of physicochemical and ADME properties**

The pharmacokinetics (ADME) and physicochemical properties of the phytocompounds from *H. indicus* (L) R.Br. was assessed using the SwissADME online tool (http://www.swissadme.ch/) and observed results were presented in Table 3. The molecular weights of top-scored phytocompounds, Hemidescine, Beta-Amyrin, Quercetin and standard drug CPUY192018 are 650.84.38 $g.mol^{-1}$, 426.72 $g.mol^{-1}$, 302.24 $g.mol^{-1}$ and 614.64 $g.mol^{-1}$, respectively, as shown by the data in Table 3, which was determined to be contrary to Lipinski's rule of five because the molecular weights of all top scored phytocompounds and standard drug are higher (MW > 350). The polar surface areas of the top-scored three phytocompounds, Hemidescine, Beta-Amyrin, Quercetin and standard drug CPUY192018 are 131.14Å², 20.23Å², 131.36Å², and 184.58Å², respectively. The predicted results also demonstrated a low rate of gastrointestinal (GI) absorption in human for the bioactive substances Hemidescine, and Beta-Amyrin, while quercetin showed better gastrointestinal (GI) absorption. The higher number of H-bonds, the more likely they are engaged in protein-ligand interaction. Hemidescine, Beta-Amyrin and Quercetin are the phytocompounds found in the

target plant, and are therefore more likely to develop into a drug-like candidate with potential Keap1-kelch inhibitors. The phytocompounds Hemidescine, Beta-Amyrin and Quercetin were shown to have synthetic accessibility scores of 8.01, 6.04, 3.23, respectively, indicating that they are challenging to synthesis.

Table 3
Toxicity profile of top scored compounds with standard drug CPUY192018.

Compound	AMES toxicity	Max. tolerated dose (human)	hERG inhibition	LD50	Hepatotoxicity	Carcinogenicity	Skin Sensitisation	*T. pyriformis* toxicity	Minnow toxicity
Hemidescine (CID: 101664025)	No	-1.41	No	2.442	No	No	No	0.286	0.714
Beta-Amyrin (CID: 73145)	No	+ 0.33	No	2.139	No	No	No	0.599	-2.344
Quercetin (CID: 5280343)	Yes	+ 0.984	No	2.251	No	No	No	0.418	2.487
CPUY192018 (CID: 73330369)	No	+ 0.52	No	1.841	Yes	No	No	0.286	-0.527

Figure 4 shows the bioavailability radar plots of the top scored phytocompounds Hemidescine, Beta-Amyrin, and Quercetin and standard CPUY192018 and their drug-like properties. The pink zone within the hexagon signifies the optimal range for the compounds. The drug-like compound's recommended range was insaturation (INSITU): fraction of carbons in the sp3 hybridization not less than 0.25, insolubility (INSOLE): log S not higher than 6, hydrophobicity (LIPO): between − 0.7 and + 5.0, rotatable bonds (FLEXI): no more than 9 rotatable bonds, molecular weight (SIZE): between 150 and 500 g.mol-1, polar surface area (POLAR): between 20 and 130 $g.mol^{-1}$ and polar surface area (POLAR): between 20 and 130 $Å^2$. The red slanted hexagon off-shoot of the vertex displays drug-like properties of the phytocompounds Hemidescine, Beta-Amyrin, and quercetin and standard CPUY192018 (Fig. 4). Moreover, using an egg-boiled model, the pharmacokinetic characteristics of the top scored phytocompounds, Hemidescine, Beta-Amyrin, Quercetin and standard CPUY192018 were examined. The egg-boiled model proved helpful in predicting two important pharmacokinetic characteristics at the same time, namely, passive gastrointestinal absorption (HIA) and blood-brain barrier (BBB) penetration. The chemical in the yolk (i.e., yellow area) indicates BBB permeation very likely, whereas albumin (i.e., white region) represents highly possible HIA absorption in the egg-shaped organization plot. The bioactive components, Hemidescine, Beta-Amyrin, and standard CPUY192018 were detected outside the boiled egg in Fig. 5, indicating poor gastrointestinal absorption, while, Quercetin was detected in the white region and higher gastrointestinal absorption. The top-scored phytocompounds Hemidescine, Beta-Amyrin, and Quercetin has significant potential to be a drug-like agents for Keap1-kelch inhibitors and used for oxidative induced diseases, as indicated by the above-mentioned expected findings.

Analysis Of Toxicity

The *in-silico* toxicity prediction of the top-scoring phytocompounds, Hemidescine, Beta-Amyrin, Quercetin, and the standard drug CPUY192018, was evaluated using the pkCSM-pharmacokinetics web-based platform. The results of the top-scoring compounds of *H. indicus* (L) R.Br. were shown in Table 4 for the predictions for AMES toxicity, drug-induced hERG toxicity, LD_{50} (median fatal dosage), hepatotoxicity, skin sensitization, Tetrahymena pyriformis (TP) toxicity, and minnow toxicity. According to the findings, there were no adverse effects, such as hepatotoxicity, carcinogenicity, or skin sensitization, for the bioactive substances Hemidescine and Beta-Amyrin. The instant or acute toxicity of compounds that were found to be the most effective during the exploration is specified by the LD_{50}.

Table 4. EHOMO and ELUMO and ΔE values of selected top binding scored compounds and standard drug CPUY192018.

Compound Name	HOMO	E_{HOMO} (ev)	LUMO	E_{LUMO} (ev)	Energy gap (Δev)
Hemidescine	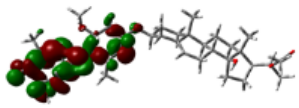	-9.5378	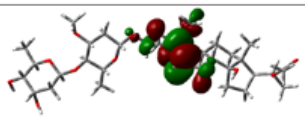	-4.4741	5.0637
Beta Amyrin	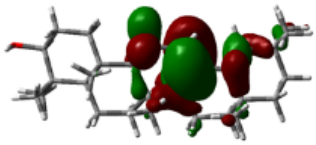	-9.8576	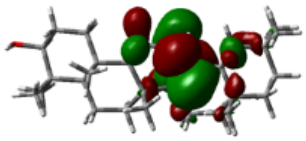	-4.6115	5.2460
Quercetin	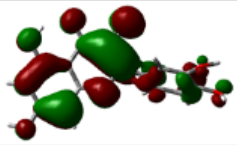	-8.4817	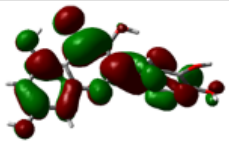	-5.3682	3.1135
Standard drug (CPUY192018)	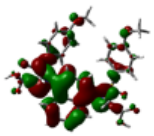	-8.5658	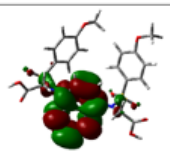	-5.9731	2.5927

Molecular Dynamics (Md) Simulation

The molecular docking calculations were followed by MD simulation of the Hemidescine, Beta-Amyrin, quercetin, and the standard drug CPUY192018 complexed with Kelch-Neh2 complex protein. The MD trajectory events of HEM- Kelch-Neh2 complex exposed that the protein RMSD fluctuated between 3.4 Å and 3 Å (Fig. 6a). Ligand RMSD was stable and fluctuation were in between 3.2 to 2 Å. Smaller RMSD fluctuation show the stability of the HEM binding Kelch-Neh2 complex. The protein-ligand contacts of HEM-Kelch-Neh2 complex revealed that amino acid residue ARG326X (84%), VAL561X (58%), LEU365X (32%), ILE416X (97%), ARG415X (65%) and VAL606X (20%) contributes maximum interaction with Hemidescine for its activity (Fig. 8a, b). The MD trajectory events of BET-Kelch-Neh2 complex exhibited that protein RMSD fluctuated initially up to 2.5 Å and retain its stability thereafter till the end with 1.2 Å (Fig. 7b). Ligand RMSD was stable and fluctuation were in between 3.2 to 2.2 Å. The protein-ligand contacts of Beta-Amyrin- Kelch-Neh2 complex revealed that amino acid residue ARG415X (41%) and GLU79P (46%) contributes maximum interaction with Beta-Amyrin for its stability and activity (Fig. 9a, b). Further, the MD trajectory events of QUE-Kelch-Neh2 protein complex showed that protein RMSD fluctuated initially up to 2.25 Å and retain its stability thereafter till the end with 1 Å (Fig. 7c). Ligand RMSD was stable and fluctuation were in between 2.2 to 1 Å. The protein-ligand contacts of QUE-Kelch-Neh2 protein complex revealed that amino acid residue GLY367X (46.4%), VAL606X (51%), VAL512X (44%), VAL418X (69%), VAL463 (81%), ARG415X (58%), and LEU365X (35%) contributes maximum interaction with Quercetin for its stability and activity (Fig. 10a, b). The MD trajectory events of standard drug CPU-Kelch-Neh2 protein complex showed that protein RMSD fluctuated initially up to 2 Å and retain its stability thereafter till the end with 1 Å (Fig. 7d). Ligand RMSD was stable and fluctuation were in between 2.6 to 2.2 Å. The protein-ligand contacts of standard CPU-Kelch-Neh2 protein complex revealed that amino acid residues VAL561X (64%), VAL514X (62%), VAL604X (49%), VAL606X (81%) and VAL418X (54%) contributes maximum interaction with standard drug CPUY192018 for its stability and bioactivity (Fig. 11a, b). RMSF analysis of all complex shows no major fluctuation due to the binding of amino acids with the key functional groups of ligands (Fig. 14). Collectively, it was noted that interaction at VAL561X, VAL606X, VAL463, ILE416X, and ARG415 are the key interacting residues for the stability and inhibition of ligands-Kelch-Neh2 protein complex. Hydroxy substitution plays a major role in interacting with key amino acids. Timeline representations (H-bonds, Hydrophobic, Ionic, water bridges) of all the amino acid residues were also observed in Fig. 15. The darker lines indicated that the continuous interactions with the target. These all the interactions made the protein-ligand complex stable throughout the entire duration of MD simulation study. Our analysis shows that HEM, BET and QUE are an appropriate candidate for additional *in vitro* testing for Kelch-Neh2 protein inhibition, as well as a framework for future lead optimization.

Density Functional Theory

DFT explored the relationship between geometry and electronic properties of chemical compounds. HOMO (highest occupied molecular orbital) is a fundamental indicator of a compound's ability to donate electrons, the frontier-orbital energies (HOMO & lowest unoccupied molecular orbital (LUMO) of phytocompounds are crucial for biological processes. The chosen phytocompounds HEM, BET, QUE, and standard medication (CPU) had their energies and HOMO-LUMO energy gaps evaluated using the B3LYP level with the 6-311G (d, p) basis set. Table 5 displays the HOMO-LUMO diagram. The standard medication (CPU) had a HOMO-LUMO energy gap of 2.5927, whereas BET had the greatest HOMO-LUMO energy gap among the phytocompounds at 5.2460, followed by HEM at 5.0637 and QUE at 3.1135. The energy gap measurements revealed that all three selected phytocompounds are both extremely stable in nature.

Discussion

Free radicals possess unpaired electrons and are closely connected to the intracellular oxidative stress, while antioxidants are reducing agents that limit oxidative stress via donating electrons to free radicals (26). Free radicals are unavoidable by-products generated during the normal cellular metabolism (27). Once developed, these radicals may cause severe damage when in contact with important cellular organelles, including nucleic acids (DNA and RNA), proteins and the cell membrane (28). These free radicals interact with the antioxidants, which can eventually neutralize them before cause damages. Plants produce numerous active phytocompounds as secondary metabolites, and many of them are act as antioxidants (29). Therefore, the present study was undertaken to evaluate the antioxidant potential of aqueous methanolic extract from *H. indicus* (L) R.Br., through DPPH, ABTS, FRAP radical scavenging assays. The investigation further extended to predict potential Keap1 inhibitors from *H. indicus* (L) R.Br., through structure based *in silico* molecular docking tools. Keap1/Nrf2 signalling is a pathway that activates the collection of over 200 genes that involves for antioxidant enzymes, cytoprotective genes, and xenobiotic transporters (30). Therefore, Keap1 is an important drug target for oxidative stress induced chronic diseases. Here, Keap1 inhibitors are potential drug candidate for oxidative stress-induced diseases including cancer, diabetes, and neurodegenerative diseases. Sixty-nine phytocompounds were identified from target plant *H. indicus* (L) R.Br. through IMPPAT database.

DPPH and ABTS assays are commonly used to measure the antioxidant potentials of pure compounds/crude extracts in *in vitro* (31). The DPPH radical is a dark violet colour in solution, when it is neutralized and transformed into DPPH-H, and it loses its colour or becomes pale-yellow. There are numerous reports of plant extracts neutralizing DPPH radicals *in vitro*. The aqueous methanolic extract of *H. indicus* (L) R.Br. showed scavenging of DPPH radical production in a concentration-dependent manner. A similar result has observed with the aqueous methanolic extract of *Azolla microphylla* earlier (32). The ABTS cation radical is generated by oxidation of ABTS by potassium persulphate. This radical cation is blue in colour and absorbs light at 734 nm. The ABTS cation radicals are reduced in the presence of hydrogen-donating antioxidants, including phenols, vitamin C and thiols (33). In the present study, 100 µg mL^{-1} of methanolic extract of *H. indicus* (L) R.Br. displayed 78.783 ± 0.24% reduced ABTS cation radicals. Further, FRAP assay is a simple, fastest and cost-effective method used to measure the antioxidant potential of plant extracts (34). The aqueous methanol extract of *H. indicus* (L) R.Br. showed a concentration-dependent manner in FRAP. In general, phenolic and flavonoid compounds in extract might be acts as antioxidants and helps to scavenge the free radical generation. The observed results indicate that the aqueous methanol extract of *H. indicus* (L) R.Br. is a probable antioxidant agent for further drug development against oxidative stress-induced diseases.

Further, the study extended to predict significant antioxidant compounds against oxidative stress-induced complications from the target plant *H. indicus* (L) R.Br. through pharmacoinformatics analysis. Currently, the use of information technology to determine the binding datasets of small molecules with known receptors is a major component for lead identification processes. Pharmacoinformatics is a collection of computer-based drug design tools including structure-based screening of compounds based on their binding affinities, pharmacokinetics, and pharmacodynamic abilities (35). Pharmacoinformatics tool helps to narrow down the synthetic and biological steps, and it has speed up the drug development processes (36). This tool also helps to understand how phytocompound bind in the active site of receptor protein, interactions amino acids, and inhibit/stimulate a certain protein might help researchers to find treatment possibilities for certain disease conditions (7). In general, the phytocompounds obtained from plants are safe, cytoprotective, cos-effective reduce/neutralize the toxins and maintain the level of ROS in cells (37). Here, a total of sixty-nine phytocompounds were selected from *H. indicus* (L) R.Br. through IMPPAT database. *In silico* molecular docking aims in the most precise prediction and the interaction between receptor and ligand molecules for potential lead discovery. All the chosen compounds docked against the Keap1 protein and noted the binding affinities between − 4.6 Kcal mol^{-1} to -11.3 Kcal mol^{-1}. Based on the binding affinities and interaction between ligand with target protein three compounds namely, Hemidescine (− 11.30 Kcal mol^{-1}), Beta-Amyrin (− 10.00 Kcal mol^{-1}), and Quercetin (− 9.80 Kcal $mol^{-1)}$ and standard drug CPUY192018 (− 9.10 Kcal mol^{-1}) were selected.

Therapeutic efficacy of the plant-derived phytocompounds mainly depends on their pharmacokinetics (ADMET), pharmacodynamics (mechanism of compounds action) and physicochemical properties (molecular weight, number of rotatable atoms, number of hydrogen bond acceptors and donors, molar refractivity, TPSA (topological polar surface area), solubility, gastrointestinal absorption, blood-brain

barrier penetration, etc.,), which are considered in the novel discovery process (38). A few crucial factors to enhancing dietary phytochemicals bioactivity and health promotion include their bioavailability to target cells, as well as human body absorption and metabolism (39). The Lipinski rule of Five is most commonly used to determine whether a phytocompounds has a particular pharmacological or biological action that qualifies it as a drug that can be taken orally by humans (40). According to the rule, a compound with molecular weight (Mw) < 500 Da, calculated logP < 5, hydrogen-bond donors < 5, hydrogen-bond acceptors < 10 and TPSA < 140 $Å^2$ will be further investigated as a potential drug because it may lose important properties related to its absorption, distribution, metabolism, and excretion (41). In the present study the top scored hits, two compounds (Hemidescine and Beta-Amyrin) only one violation of parameter and third compound, Quercetin not violated any of the Lipinski's rule of five. While compared with standard drug CPUY192018 has showed two parameters violated in the Lipinski's rule of five. Phytochemicals are naturally occurring substances that can be found in a variety of plants that are consumed by humans and are generally thought to be safe. Since most phytochemicals have not recognized potential for harm, the Food and Drug Administration (FDA) in the United States does not impose restrictions on their use (42).

Prior to the lead identification, the *in-silico* toxicity prediction studies provide information on the cellular, organ and tissue toxicity profile of the compounds, which reduces cost and time as well as minimizing the rate of late-stage rejection in a drug discovery process (43). Also, toxicity testing connected with pharmacokinetic and pharmacodynamic features must be studied in order for a lead compound to be approved for commercial usage (44). The availability of potentially beneficial drugs for human use gets delayed, because animal research has high costs and delays in drug approval (45). Computer-aided methods for predicting the toxicity of phytocompounds are therefore recognized as useful (46). In the present study, the toxicity results revealed that all selected top hits had no harmful effects. The LD_{50} (median fatal dosage) notified the immediate or acute toxicity of substances that were determined to be the most effective in the investigation. The stability of molecular docking results of the protein-ligand complexes was explored through molecular dynamics simulation studies. All three protein-ligand complexes were validated by interpreting the RMSD, RMSF, hydrogen bonding, and interacting amino acids of the protein with lead phytochemical complexes and were found to be stable during the simulation.

Experimental Section

Plant materials and reagents

Hemidesmus indicus (L) R.Br. "Indian Sarsaparilla" was collected from the foothills of Western Ghats in and around Kilavankoil Hills (longitude: 77.5232° and latitude: 9.6383°), Virudhunagar district, India during the early winter season. The root portion of the collected plant was separated with the help of fine knife. Later, the separated root repeatedly cleaned by tap water to remove soil and other debris, then dried naturally for 72 h, and then ground into a fine powder. The grounded powder was screened through a 60-mesh sieve size and safely stored in a desiccator for further experiments. The fine powder was subjected to an ultrasonic-assisted extraction (UAE). Extraction was performed in an adjustable ultrasonic bath using 5 g fine powdered sample of H. indicus (L) R.Br. along with 50 mL of methanol (80%) at specified ultrasound intensity (60 W cm − 2), pulse cycle (0.2 seconds) and temperature (40°C) for 20 min. UV–Visible spectrophotometer of Shimadzu UV-1800 series, UV Probe 2.62 software, Japan, was utilized for the analysis. Rotary vacuum dryer (Rotavapor, Buchi India Pvt, Ltd., India) and mixer grinder (Premier Electronics Ltd., India) were also used in this study. A sensitive colorimetric scavenger 2,2-diphenyl-1-picrylhydrazyl (DPPH) and 2,2'-Azinobis (3-ethylbenzothiazoline-6-sulphonic acid) radical cation (ABTS) assay adapted were from Sigma-Aldrich, MO, USA. Methanol, 2,4,6-tripyridyl-s-triazine (TPTZ), rutin and gallic acid were obtained from Himedia laboratories Pvt. Ltd., Mumbai, India.

Antioxidant Activity

DPPH radical scavenging activity

The DPPH radical scavenging activity of *H. indicus* (L) R.Br. extract was performed using DPPH reagent (4g DPPH dissolved in 90% methanol), as indicated by our previously published article with slight modification (47). Briefly, 0.1 mM DPPH solution (0.1 mM) 1 mL of freshly prepared DPPH solution was added to 3 mL of different concentrations (6.25–100 mg mL-1) of H. indicus (L) R.Br. extract and the reference drug (rutin) diluted in 90% methanol. The control was prepared as above with 3 mL of 90% methanol instead of a sample. The mixture was kept in the dark for 30 min at room temperature. All the samples were prepared in triplicates, and the absorbance was recorded at 517 nm using a UV–Visible spectrophotometer against a blank. The percentage of inhibition of DPPH was determined from the following formula:

DPPH scavenging effect (% inhibition) = (A0 − A1)/A0 × 100

where, A0 is the absorbance of the control reaction, and A1 is the absorbance in the presence of all of the extract samples and reference.

Abts Radical Scavenging Activity

This assay depends on the capacity of the acquired extract of *H. indicus* (L) R.Br. sample to scavenge 2,2'-azino-bis(ethylbenzthiazoline-6-sulfonic acid (ABTS) radical cation (48). The ABTS radical cation was generated by the interaction between 7 mM of ABTS salt solution and 2.45 mM potassium per sulphate solution (1/1, v/v) held in the dark at room temperature for 12–16 h. The created ABTS solution was carefully mixed with 0.1 mL of plant extract after being diluted with 0.3 mL of methanol. After 6 min, the reaction mixture was incubated, and a UV-visible spectrophotometer was used to measure the absorbance at 734 nm, which was set to 0.700 (0.0020). Rutin in 80% methanol was used as the reference standard, and the standard curve was used to calculate the percentage of ABTS scavenging activity.

ABTS scavenging effect (% inhibition) = (A0 − A1)/A0 × 100

where, A0 is the absorbance of the control reaction, and A1 is the absorbance in the presence of all of the extract samples and reference.

Ferric Reducing Antioxidant Potential (Frap) Assay

The antioxidant capacity of *H. indicus* (L) R.Br. extract was calculated spectrophotometrically by the method of Benzie and Strain (49), and a technique improved by Pulido et al. (50). The method depends on the reduction of Fe^{3+} TPTZ (colourless complex) to Fe^{2+} tripyridyltriazine (blue coloured complex) generation by the action of electron donating antioxidants at low pH. The change in absorbance at 593 nm is used to track this process. At pH 3.6, 300 mM acetate buffer (3.1 g sodium acetate, 16 mL acetic acid), 10 mM TPTZ (2,4,6-tripyridyl-s-triazine) solution in 40 mM hydrochloric acid solution, and 20 mM $FeCl_3.6H_2O$ solution were used to make the FRAP reagent. A mixture of the acetate buffer (25 mL), TPTZ (2.5 mL), and $FeCl_3$ was then added (2.5 mL). After 30 min of incubation at 37°C, the newly generated FRAP solution was allowed to react with the extract from *H. indicus* (40 µL) before the absorbance was measured at 593 nm. The $FeSO_4$ standard was linear between 200 and 1000 µM. Results expressed in µM Fe(II) g^{-1} dry mass were compared to a standard, ascorbic acid.

In silico **study**

Ligand Library Preparation

Sixty-nine known phytochemicals from the *H. indicus* (L) R.Br. was identified from the Indian Medicinal Plants, Phytochemistry and Therapeutics (IMPPAT) database (51). The primary phytochemicals chosen were sterols, alkaloids, and flavonoids. For *in silico* molecular docking experiments, the three-dimensional structures (Structure Data File format) of chosen phytocompounds were drawn using Chemsketch software and energy-optimized through MMFF94 (Merck molecular force field 94), and a ready-to-dock library was prepared in BIOVIA discovery studio software packages. The standard Keap1 protein inhibitor, CPUY192018 (PubChem CID: 73330369) was used to compare the inhibitory effect of the selected plant-based phytocompounds.

Target Protein Preparation

The three-dimensional X-ray crystal structure of Kelch-Neh2 complex protein (PDB entry ID: 2flu, resolution 1.50 Å) was retrieved from the RCSB PDB (Research Collaboratory for Structural Bioinformatics, Protein Data Bank, https://www.rcsb.org/) website (52). Using the Swiss-PDB Viewer v4.1.0, incorrect bonds and side chain anomalies were fixed, and missing residues were added to the recovered protein (53). The file was assigned the name target.pdb which was then saved for further investigation. Additionally, we defined the protein structure and amino acid position from active sites using BIOVIA Discovery Studio Visualizer version 4.0 software (Accelrys Software Inc., San Diego, CA, USA), which was subsequently used for the molecular docking studies.

Investigation Of Protein-ligands Interaction

Active Binding Site Prediction

The discovery of structure-based lead phytocompounds and the understanding of protein function are two areas where predicting ligand binding sites from specific protein structural locations has significant implications. This indicated binding region helps in the lead phytocompounds ability to bind and establish a strong interaction with the target protein in order to provide the most effective and

advantageous catalytic effects. For further research, all potential active binding sites of the targeted phytocompounds were identified using the PrankWeb (https://prankweb.cz) online tool (54).

Molecular Docking

Using the PyRx 0.8 tool in the AutoDock Vina program, a receptor grid box was generated once the target protein active binding site was predicted (55). The created ready-to-dock phytochemicals library was docked against chosen Kelch-Neh2 complex protein (PDB ID: 2flu) to explore the ligand-protein interactions (56). The grid box with a 10.0 radius across the active binding site of the predicted area was selected to assess the molecular binding affinities (Kcal mol^{-1}) using the protein (receptor) and phytocompounds (ligand) files stored in the ".pdbqt" format. The binding energy affinities of up to 10 different docking sites for each ligand were assessed using the AutoDock Vina tool. After docking, phytochemicals with best and top conformation were determined based on their Root-Mean-Square Deviation (RMSD) and S-score binding affinity values. The best docked complexes were visualized by the Discovery Studio Visualizer tool to analyze the protein-ligand complex structures, with interactions (2D and 3D plots), the number of hydrogen bonds, hydrophobic bonds and noncovalent interactions for each complex.

Drug-likeness Evaluation

The evaluation of the drug-likeness, pharmacokinetics, and toxicity profile of the drug candidate is a significant step in the drug discovery process. Here, we investigated pharmacokinetics (absorption, distribution, metabolism, and excretion), toxicity and some physicochemical properties of the top-scored phytocompounds, such as molecular weight, octanol-water partition coefficient log P (LogP), the number of hydrogen bond acceptors, hydrogen bond donors, solubility, molar refractivity, gastrointestinal absorption and blood-brain barrier penetration using Swiss-ADME (57) and pkCSM-pharmacokinetic online web-based tools (58) of the selected phytocompounds from *H.indicus* (L) R.Br.

Molecular Dynamics Simulation Studies

The DESMOND computer programme was developed by the D.E. Shaw research group to compute molecular dynamics (MD) simulation of protein-ligand complexes (PLC) (59). Through MD simulation modelling, the potential effects of PLC at target binding sites in physiological situations are emphasized (Academic license, Version 2020-1, Schrödinger, LLC, New York, NY, 2021-4, Schrödinger Release: QikProp). **The panel for system developers**: At this initial stage, the panel enables us to construct a box (10 x 10 x 10) holding water molecules and physiological features like pH (60). To meet the specific requirements of the study procedure, Na + or Cl- ions can be introduced if the pH is not present or if it needs to be raised or lowered. The simple orthorhombic point-charge (SPC) water model was used to solve the docked protein-ligand complexes. The physiological salt concentration was maintained at 0.15 M while the solvated system was neutralized using counter ions. The OPLS AA (Optimal Potentials for Liquid Simulation - All Atom) force field was applied to the PLC system (61). **Minimization**: A moderate minimization will be performed at roughly 100 ps on the ready PLC with the help of the system builder panel. As a result, the prepared system stabilizes in response to its surroundings. Reversible Reference System Propagator Algorithms (RESPA) integrator (62), Martyna-Tobias-Klein barostat, and the Nose-Hoover chain thermostat were all employed in molecular dynamics with two ps relaxation durations(63). The final version of the MD simulation was created using the equilibrated system. The MD simulation was run for 100 ns at 310.15 K temperature and 1.0 bar pressure using the NPT (Isothermal-Isobaric ensemble, constant temperature, constant pressure, and constant number of particles) ensemble with the default relaxation parameters (64). Once the simulation is complete, the findings are analyzed using a simulation interaction diagram (65).

Density Functional Theory (Dft)

The electronic properties of the drug-like compounds played a crucial role in its pharmacological activity. The three-dimensional electronic density system may be used to measure the electronic states of atoms, molecules, and solids using the DFT theory. DFT's primary objective is to use the basic principles of quantum mechanics to create a quantitative knowledge of material qualities. The Gaussian 03W software and the GaussView molecular visualization tools were used for computational computations in this work to determine the top binding scored bioactive chemicals acquired from molecular docking. The molecular structures of the chosen bioactive compound were optimized using the DFT/Becke-3-Lee-Yang-Parr (B3LYP) method using a 6-311G (d.p) basis set. Using the optimized structures, the frontier molecular orbital energies of the chosen bioactive compounds were determined, including their energy gaps (Eg) and lowest unoccupied molecular orbitals (ELUMO) and highest occupied molecular orbitals (EHOMO). GaussView, a molecular visualization programme, was used to depict the molecular orbital energy diagrams that were produced for the chosen bioactive chemicals (66).

Conclusions

Plants and plant-based products consist of an array of antioxidant phytocompounds crucial for preventing and treating many chronic diseases. Nrf2 is a central transcription factor in oxidative stress responses and is connected to numerous chronic diseases, and it is activated after dissociating from the Keap1. This study explored the quantification of free radical scavenging potential from *H. indicus* (L) R.Br. aqueous methanolic extract and found significant Keap1 inhibitors from this target plant via in silico molecular docking and molecular dynamics simulation studies. Through a thorough molecular docking investigation of phytocompounds, the top three scored phytocompounds (Hemidescine, Beta-amyrin and Quercetin) were selected on the basis of least/better binding affinities than standard Keap1 inhibitor (CPU192018). In addition, the molecular dynamics simulation studies exhibited that top-scored three compounds with Keap1 protein complexes were highly stable during the entire simulation period. Moreover, pharmacokinetics and physicochemical properties confirm the drug-likeness and safety profiles of three selected phytocompounds. These studies further confirmation of antioxidant activity and effective inhibition of Keap1 protein against oxidative stress induced health complications. Additional *in vitro* and *in vivo* animal studies are necessary to evaluate the Keap1 protein inhibition and Nrf2 protein activation of these phytocompounds.

Declarations

Acknowledgements

The authors are grateful to the Management of Kalasalingam Academy of Research and Education, Krishnankoil, India, for research fellowships and utilizing research facilities.

Author contributions

SK contributed to the study conception and design. SV, PP, CP, SJK, SRK and SK performed computational simulation and analysed the data. SV, SRK and SK wrote the original manuscript. SRK, SJK and SK proofread the manuscript. All the authors have read and approved the manuscript for submission.

Conflict of interest

The authors declare that they have no known competing financial interests or personal relationships that could have appeared to influence the work reported in this paper.

Ethical approval

None of the authors conducted any human or animal experiments for this publication.

References

1. Saccomano SC, Cash KJ. A near-infrared optical nanosensor for measuring aerobic respiration in microbial systems. Analyst. 2022;147(1):120-9. https://doi.org/10.1039/D1AN01855H
2. Koltover VK. Reliability and Longevity of Biological Systems: The Free-Radical Redox Timer of Aging. Redox Signaling and Biomarkers in Ageing: Springer; 2022. p. 21-44. https://doi.org/10.1089/ars.2013.5228
3. Martemucci G, Costagliola C, Mariano M, D'andrea L, Napolitano P, D'Alessandro AG. Free Radical Properties, Source and Targets, Antioxidant Consumption and Health. Oxygen. 2022;2(2):48-78. https://doi.org/10.3390/oxygen2020006
4. Mohan UP, Sriram B, Panneerselvam T, Devaraj S, MubarakAli D, Parasuraman P, et al. Utilization of plant-derived Myricetin molecule coupled with ultrasound for the synthesis of gold nanoparticles against breast cancer. Naunyn Schmiedebergs Arch Pharmacol 2020;393(10):1963-76. https://doi.org/10.1007/s00210-020-01874-6
5. Kalimuthu AK, Panneerselvam T, Pavadai P, Pandian SRK, Sundar K, Murugesan S, et al. Pharmacoinformatics-based investigation of bioactive compounds of Rasam (South Indian recipe) against human cancer. Sci Rep. 2021;11(1):1-19. https://doi.org/10.1038/s41598-021-01008-9
6. Aggarwal V, Tuli HS, Varol A, Thakral F, Yerer MB, Sak K, et al. Role of reactive oxygen species in cancer progression: molecular mechanisms and recent advancements. Biomolecules. 2019;9(11):735. https://doi.org/10.3390/biom9110735
7. Palanichamy C, Pavadai P, Panneerselvam T, Arunachalam S, Babkiewicz E, Ram Kumar Pandian S, et al. Aphrodisiac Performance of Bioactive Compounds from Mimosa pudica Linn.: In Silico Molecular Docking and Dynamics Simulation Approach. Molecules 2022;27(12):3799. https://doi.org/10.3390/molecules27123799

8. Rodriguez-Enriquez F, Torres I, Vina D. Natural products for the treatment of Alzheimer's disease: present and future expectations. Front Clin Drug Res CNS Neurol Disorders 2017;5:74-170. https://doi.org/10.2174/9781681085852117050005
9. Adwas AA, Elsayed A, Azab A, Quwaydir F. Oxidative stress and antioxidant mechanisms in human body. J Appl Biotechnol Bioeng 2019;6(1):43-7. https://doi.org/110.15406/jabb.2019.06.00173
10. Santovito G, Trentin E, Gobbi I, Bisaccia P, Tallandini L, Irato P. Non-enzymatic antioxidant responses of Mytilus galloprovincialis: Insights into the physiological role against metal-induced oxidative stress. Comparative Biochemistry and Physiology Part C: Toxicol Pharmacol 2021;240:108909. https://doi.org/10.1016/j.cbpc.2020.108909
11. Kunjiappan S, Bhattacharjee C, Chowdhury R. Hepatoprotective and antioxidant effects of *Azolla microphylla* based gold nanoparticles against acetaminophen induced toxicity in a fresh water common carp fish (Cyprinus carpio L.). Nanomed 2015, 2(2): 88-110.
12. Mehla N, Chhajer AK, Kumar K, Dahiya S, Mohindroo V. Applications of Antioxidants: A Review 13. Plant Antioxid Health 2022:313. https://doi.org/10.1007/978-3-030-45299-5_28-1
13. Zhang J, Duan D, Song ZL, Liu T, Hou Y, Fang J. Small molecules regulating reactive oxygen species homeostasis for cancer therapy. Med Res Rev 2021;41(1):342-94. https://doi.org/10.1002/med.21734
14. Pickering RJ, Rosado CJ, Sharma A, Buksh S, Tate M, de Haan JB. Recent novel approaches to limit oxidative stress and inflammation in diabetic complications. Clin Transl Immunol 2018;7(4):e1016. https://doi.org/10.1002/cti2.1016
15. Kang Q, Yang C. Oxidative stress and diabetic retinopathy: Molecular mechanisms, pathogenetic role and therapeutic implications. Redox Biol 2020;37:101799. https://doi.org/10.1016/j.redox.2020.101799
16. Tonelli C, Chio IIC, Tuveson DA. Transcriptional regulation by Nrf2. Antioxid Redox Signal 2018;29(17):1727-45. https://doi.org/10.1089/ars.2017.7342
17. Baird L, Yamamoto M. The molecular mechanisms regulating the KEAP1-NRF2 pathway. Mol Cell Biol 2020;40(13):e00099-20. https://doi.org/10.1128/MCB.00099-20
18. Hayes AJ, Skouras C, Haugk B, Charnley RM. Keap1–Nrf2 signalling in pancreatic cancer. Int J Biochem Cell Biol 2015;65:288-99. https://doi.org/10.1016/j.biocel.2015.06.017
19. Tao S, Liu P, Luo G, Rojo de la Vega M, Chen H, Wu T, et al. p97 negatively regulates NRF2 by extracting ubiquitylated NRF2 from the KEAP1-CUL3 E3 complex. Mol Cell Biol 2017;37(8):e00660-16. https://doi.org/10.1128/MCB.00660-16
20. Deshmukh P, Unni S, Krishnappa G, Padmanabhan B. The Keap1–Nrf2 pathway: promising therapeutic target to counteract ROS-mediated damage in cancers and neurodegenerative diseases. Biophys Rev 2017;9(1):41-56. https://doi.org/10.1007/s12551-016-0244-4
21. Vallejo MJ, Salazar L, Grijalva M. Oxidative stress modulation and ROS-mediated toxicity in cancer: a review on in vitro models for plant-derived compounds. Oxid Med Cell Longev 2017;2017. https://doi.org/10.1155/2017/4586068
22. Kumar Y, Yadav DN, Ahmad T, Narsaiah K. Recent trends in the use of natural antioxidants for meat and meat products. Compre Rev Food Sci Food Safe 2015;14(6):796-812. https://doi.org/10.1111/1541-4337.12156
23. Srivastava A, Srivastava P, Pandey A, Khanna V, Pant A. Phytomedicine: A potential alternative medicine in controlling neurological disorders. New Look to Phytomedicine: Elsevier; 2019. p. 625-55. https://doi.org/10.2174/1389200218666170710190249
24. Kawlni L, Bora M, Upadhyay SN, Mukherjee K, Hazra J. Pharmacological and therapeutic profile of anantamula (Hemidesmus indicus (L.) R. Br.): A comprehensive review. Int J Ayurveda Pharma Res 2017.
25. Turrini E, Calcabrini C, Tacchini M, Efferth T, Sacchetti G, Guerrini A, et al. In vitro study of the cytotoxic, cytostatic, and antigenotoxic profile of Hemidesmus indicus (L.) R. Br.(Apocynaceae) crude drug extract on T lymphoblastic cells. Toxins 2018;10(2):70. https://doi.org/10.3390/toxins10020070
26. Valko M, Rhodes C, Moncol J, Izakovic M, Mazur M. Free radicals, metals and antioxidants in oxidative stress-induced cancer. Chem Biol Interact 2006;160(1):1-40. https://doi.org/10.1016/j.cbi.2005.12.009
27. Gladyshev VN. The free radical theory of aging is dead. Long live the damage theory! Antioxid. Redox Signal 2014;20(4):727-31. https://doi.org/10.1089/ars.2013.5228
28. Di Mascio P, Martinez GR, Miyamoto S, Ronsein GE, Medeiros MH, Cadet J. Singlet molecular oxygen reactions with nucleic acids, lipids, and proteins. Chem Rev 2019;119(3):2043-86. https://doi.org/10.1021/acs.chemrev.8b00554
29. Russell W, Duthie G. Plant secondary metabolites and gut health: the case for phenolic acids. Proc Nutr Soc 2011;70(3):389-96. https://doi.org/10.1017/S0029665111000152
30. Raghunath A, Sundarraj K, Nagarajan R, Arfuso F, Bian J, Kumar AP, et al. Antioxidant response elements: Discovery, classes, regulation and potential applications. Redox Biol 2018;17:297-314. https://doi.org/10.1016/j.redox.2018.05.002

31. Ediriweera MK, Tennekoon KH, Samarakoon SR. In vitro assays and techniques utilized in anticancer drug discovery. J Appl Toxicol 2019;39(1):38-71. https://doi.org/10.1002/jat.3658
32. Selvaraj K, Chowdhury R, Bhattacharjee C. Isolation and structural elucidation of flavonoids from aquatic fern Azolla microphylla and evaluation of free radical scavenging activity. Int J Pharm Pharm Sci. 2013;5(3):743-9.
33. Cetin A, Geçibesler IH. Evaluation as antioxidant agents of 1, 2, 4-triazole derivatives: effects of essential functional groups. J Appl Pharm Sci 2015;5(6):120-6. https://doi.org/10.7324/JAPS.2015.50620
34. Awika JM, Rooney LW, Wu X, Prior RL, Cisneros-Zevallos L. Screening methods to measure antioxidant activity of sorghum (Sorghum bicolor) and sorghum products. J Agri Food Chem 2003;51(23):6657-62. https://doi.org/10.1021/jf034790i
35. Olğaç A, Türe A, Olğaç S, Möller S. Cloud-based high throughput virtual screening in novel drug discovery. High-performance modelling and simulation for big data applications: Springer, Cham; 2019. p. 250-78. https://doi.org/10.1007/978-3-030-16272-6_9.
36. Khan DA, Hamdani SDA, Iftikhar S, Malik SZ, Zaidi N-u-SS, Gul A, et al. Pharmacoinformatics approaches in the discovery of drug-like antimicrobials of plant origin. J Biomol Struct Dyn 2022;40(16):7612-28. https://doi.org/10.1080/07391102.2021.1894982
37. Gechev TS, Van Breusegem F, Stone JM, Denev I, Laloi C. Reactive oxygen species as signals that modulate plant stress responses and programmed cell death. Bioessays. 2006;28(11):1091-101. https://doi.org/10.1002/bies.20493
38. Ahmad K, Roouf Bhat A, Athar F. Pharmacokinetic evaluation of callistemon viminalis derived natural compounds as targeted inhibitors against δ-opioid receptor and farnesyl transferase. Lett Drug Des Discov 2017;14(4):488-99.
39. Cosme P, Rodríguez AB, Espino J, Garrido M. Plant phenolics: Bioavailability as a key determinant of their potential health-promoting applications. Antioxidants. 2020;9(12):1263. https://doi.org/10.3390/antiox9121263
40. Chen X, Li H, Tian L, Li Q, Luo J, Zhang Y. Analysis of the physicochemical properties of acaricides based on Lipinski's rule of five. J Comput Biol 2020;27(9):1397-406. https://doi.org/10.1089/cmb.2019.0323
41. Zafrani Y, Yeffet D, Sod-Moriah G, Berliner A, Amir D, Marciano D, et al. Difluoromethyl bioisostere: examining the “lipophilic hydrogen bond donor” concept. J Med Chem 2017;60(2):797-804. https://doi.org/10.1021/acs.jmedchem.6b01691
42. Zhang Y-J, Gan R-Y, Li S, Zhou Y, Li A-N, Xu D-P, et al. Antioxidant phytochemicals for the prevention and treatment of chronic diseases. Molecules. 2015;20(12):21138-56. https://doi.org/10.3390/molecules201219753
43. Di L, Kerns E. Drug-like properties: concepts, structure design and methods from ADME to toxicity optimization: Academic Press; 2015.
44. Deore AB, Dhumane JR, Wagh R, Sonawane R. The stages of drug discovery and development process. Asian J Pharm Res Dev 2019;7(6):62-7. https://doi.org/10.22270/ajprd.v7i6.616
45. Fermini B, Fossa AA. The impact of drug-induced QT interval prolongation on drug discovery and development. Nat Rev Drug Discov 2003;2(6):439-47. https://doi.org/10.1038/nrd1108
46. Rasool N, Akhtar A, Hussain W. Insights into the inhibitory potential of selective phytochemicals against Mpro of 2019-nCoV: a computer-aided study. Struct Chem 2020;31(5):1777-83. https://doi.org/10.1007/s11224-020-01536-6
47. Kalimuthu AK, Parasuraman P, Sivakumar P, Murugesan S, Arunachalam S, Pandian SRK, et al. In silico, in vitro screening of antioxidant and anticancer potentials of bioactive secondary metabolites from an endophytic fungus (Curvularia sp.) from Phyllanthus niruri L. Environ Sci Pollut Res 2022:1-18. https://doi.org/10.1007/s11356-022-19249-0
48. Ganesan V, Gurumani V, Kunjiappan S, Panneerselvam T, Somasundaram B, Kannan S, et al. Optimization and analysis of microwave-assisted extraction of bioactive compounds from Mimosa pudica L. using RSM & ANFIS modeling. J Food Measure Charac 2018;12(1):228-42. https://doi.org/10.1007/s11694-017-9634-y
49. Benzie IF, Strain JJ. The ferric reducing ability of plasma (FRAP) as a measure of “antioxidant power”: the FRAP assay. Anal Biochem 1996;239(1):70-6. https://doi.org/10.1006/abio.1996.0292
50. Pulido R, Bravo L, Saura-Calixto F. Antioxidant activity of dietary polyphenols as determined by a modified ferric reducing/antioxidant power assay. J Agric Food Chem 2000;48(8):3396-402. https://doi.org/10.1021/jf9913458
51. Mohanraj K, Karthikeyan BS, Vivek-Ananth R, Chand R, Aparna S, Mangalapandi P, et al. IMPPAT: a curated database of Indian medicinal plants, phytochemistry and therapeutics. Sci Rep 2018;8(1):1-17. https://doi.org/10.1038/s41598-018-22631-z
52. Burley SK, Berman HM, Bhikadiya C, Bi C, Chen L, Di Costanzo L, et al. RCSB Protein Data Bank: biological macromolecular structures enabling research and education in fundamental biology, biomedicine, biotechnology and energy. Nucleic Acids Res 2019;47(D1):D464-D74. https://doi.org/10.1093/nar/gky1004
53. Kaplan W, Littlejohn TG. Swiss-PDB viewer (deep view). Brief Bioinformatics 2001;2(2):195-7. https://doi.org/10.1093/bib/2.2.195
54. Jendele L, Krivak R, Skoda P, Novotny M, Hoksza D. PrankWeb: a web server for ligand binding site prediction and visualization. Nucleic Acids Res 2019;47(W1):W345-W9. https://doi.org/10.1093/nar/gkz424

55. Kumar B, Parasuraman P, Murthy TPK, Murahari M, Chandramohan V. In silico screening of therapeutic potentials from Strychnos nux-vomica against the dimeric main protease (Mpro) structure of SARS-CoV-2. J Biomol Struct Dyn 2022;40(17):7796-814. https://doi.org/10.1080/07391102.2021.1902394
56. Alamri MA, Tahir Ul Qamar M, Mirza MU, Bhadane R, Alqahtani SM, Muneer I, et al. Pharmacoinformatics and molecular dynamics simulation studies reveal potential covalent and FDA-approved inhibitors of SARS-CoV-2 main protease 3CLpro. J Biomol Struct Dyn 2021;39(13):4936-48. https://doi.org/10.1080/07391102.2020.1782768
57. Mishra S, Dahima R. In vitro ADME studies of TUG-891, a GPR-120 inhibitor using SWISS ADME predictor. J Drug Deliv Ther 2019;9(2-s):366-9. https://doi.org/10.22270/jddt.v9i2-s.2710
58. Vijayalakshmi M, Dhanapradeeba V, Kunjiappan S, Sundar K, Pandian SRK. Targeting TLRs with the Derivatives of Mimosa Pudica: An In Silico Approach. Biointerface Res Appl Chem. 2022;2023(13):3. https://doi.org/10.33263/BRIAC133.237
59. Shaw DE, Deneroff MM, Dror RO, Kuskin JS, Larson RH, Salmon JK, et al. Anton, a special-purpose machine for molecular dynamics simulation. ACM SIGARCH Comput Archit News 2007;35(2):1-12. https://doi.org/10.1145/1364782.1364802
60. Mark P, Nilsson L. Structure and dynamics of the TIP3P, SPC, and SPC/E water models at 298 K. J Phy Chem A 2001;105(43):9954-60.
61. Jorgensen WL, Maxwell DS, Tirado-Rives J. Development and testing of the OPLS all-atom force field on conformational energetics and properties of organic liquids. J Am Chem Soc 1996;118(45):11225-36.
62. Tuckerman M, Berne BJ, Martyna GJ. Reversible multiple time scale molecular dynamics. J Chem Phy 1992;97(3):1990-2001.
63. Cheng A, Merz KM. Application of the nosé– hoover chain algorithm to the study of protein dynamics. J Phy Chem 1996;100(5):1927-37.
64. Kalibaeva G, Ferrario M, Ciccotti G. Constant pressure-constant temperature molecular dynamics: a correct constrained NPT ensemble using the molecular virial. Mol Phy 2003;101(6):765-78.
65. Dessai PG, Dessai SP, Dabholkar R, Pednekar P, Naik S, Mamledesai S, et al. Design, synthesis, graph theoretical analysis and molecular modelling studies of novel substituted quinoline analogues as promising anti-breast cancer agents. Mol Diver 2022:1-20. https://doi.org/10.1007/s11030-022-10512-7
66. Saravanan G, Panneerselvam T, Kunjiappan S, Parasuraman P, Alagarsamy V, Udayakumar P, et al. Graph theoretical analysis, in silico modeling, prediction of toxicity, metabolism and synthesis of novel 2-(methyl/phenyl)-3-(4-(5-substituted-1, 3, 4-oxadiazol-2-yl) phenyl) quinazolin-4 (3H)-ones as NMDA receptor inhibitor. Drug Dev Res 2019;80(3):368-85. https://doi.org/10.1007/s00210-011-0620-3

Figures

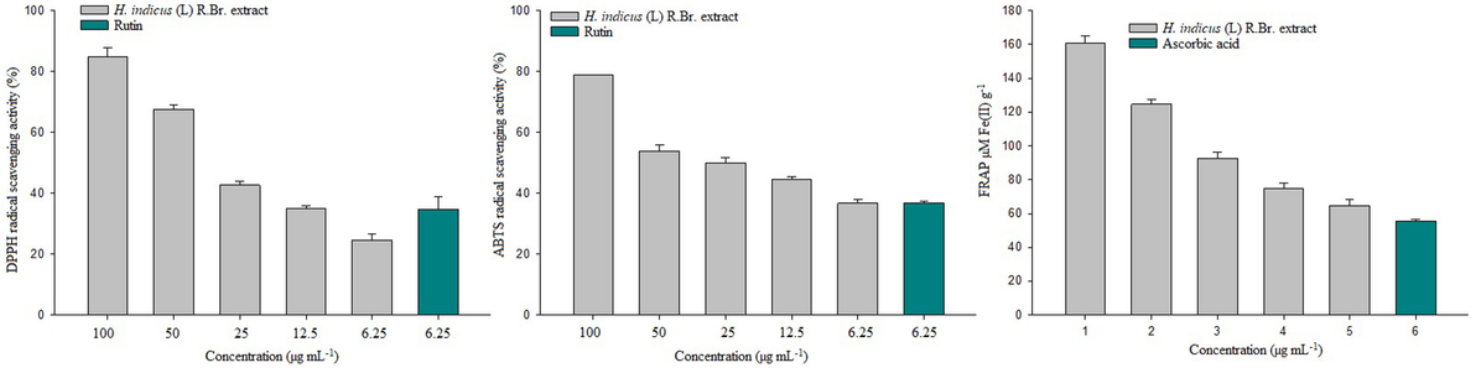

Figure 1

DPPH radical scavenging activities of various concentrations of aqueous methanolic extract of *H. indicus* (L) R.Br.(a); ABTS radical scavenging activities of various concentrations of aqueous methanolic extract of *H. indicus* (L) R.Br.(b); FRAP potential of various concentration of aqueous methanolic extract of *H. indicus* (L) R.Br.

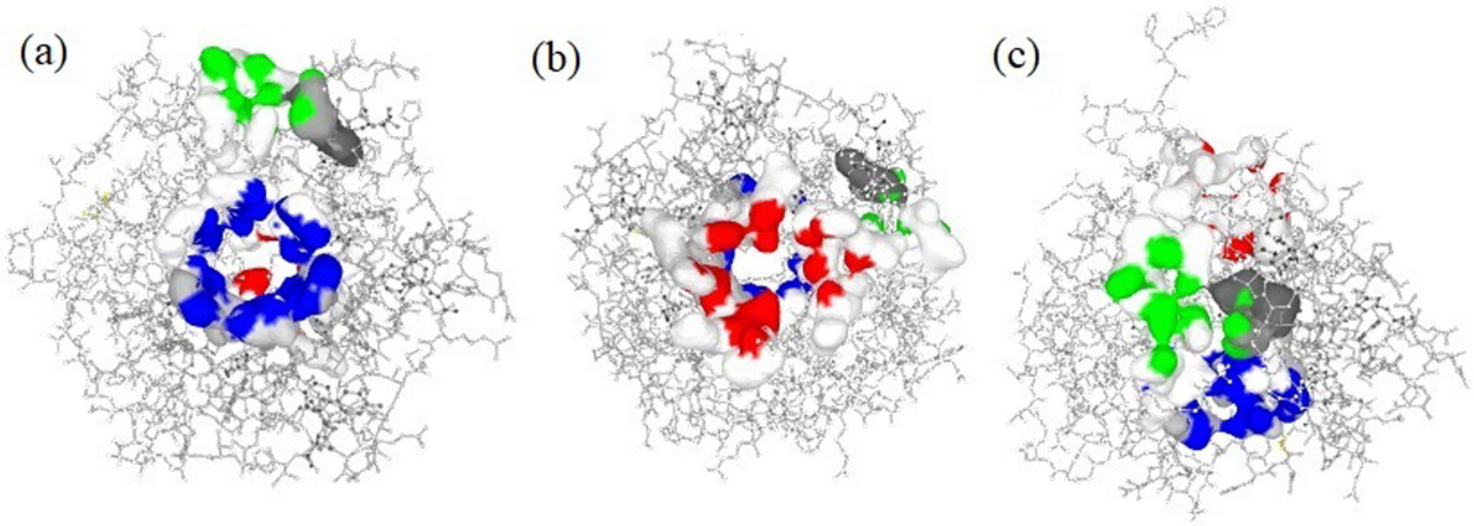

Figure 2

The PrankWeb tool is used to predict the binding pockets and correspondence binding sites of the Keap1 (Kelch-Neh2 complex) protein. Three binding pockets were predicted with different colours (blue, red, and green). The first binding pocket (blue colour) is the highest score of all three pockets, with a pocket score of 5.91, 18 amino acids, and a probability score was 0.310 (a). The second binding pocket (red colour) with a pocket score of 4.11, 14 amino acids, and a probability score was 0.176 (b). The third binding pocket (green colour) had the least pocket score of 1.21, 8 amino acids, and a probability score was 0.012 (c).

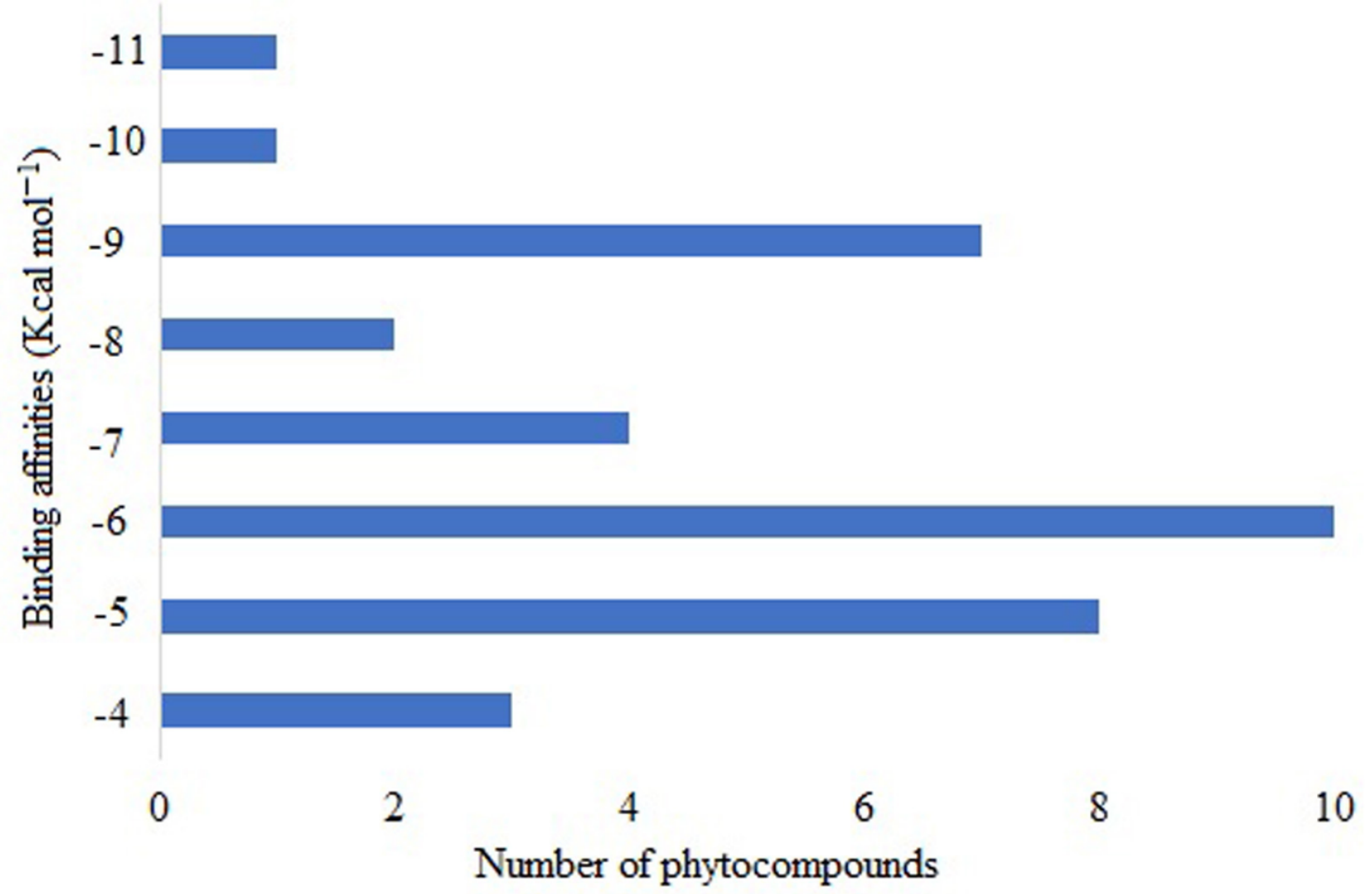

Figure 3

Showing the range of molecular docking score distribution of sixty-nine phytocompounds presence in the *H. indicus* (L) R.Br.

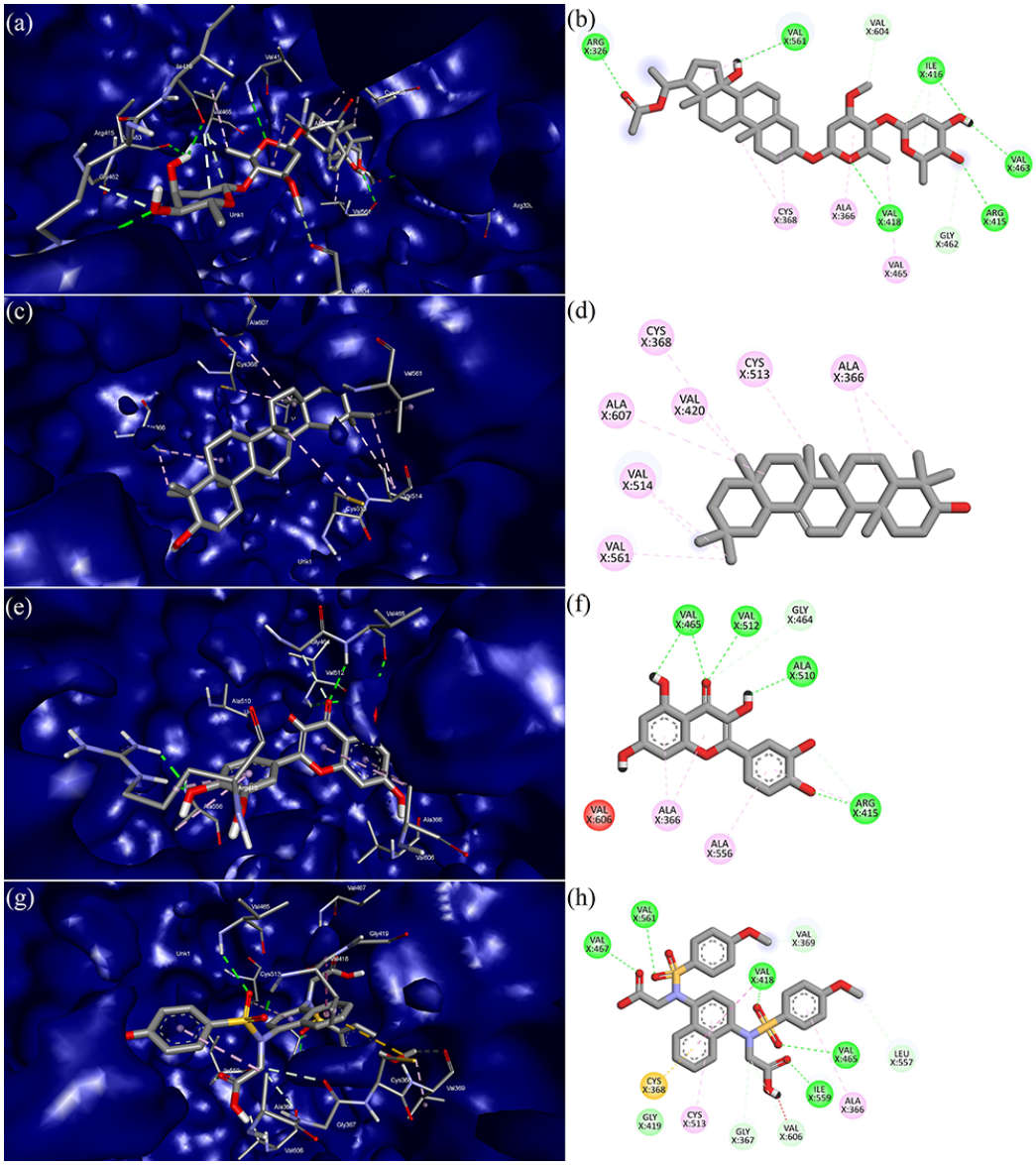

Figure 4

Depicted the interaction between the compound Hemidescine-Keap1 protein complex. Left side representing 3D and the right side representing 2D complex protein–ligand interaction (a); the interaction between the compound Beta-Amyrin-Keap1 protein complex. Left side representing 3D and the right side representing 2D complex protein–ligand interaction (b); the interaction between the compound Quercetin-Keap1 protein complex. Left side representing 3D and the right side representing 2D complex protein–ligand interaction (c); the interaction between the standard drug (CPUY192018) with Keap1 protein. Left side representing 3D and the right side representing 2D complex protein–ligand interaction (d).

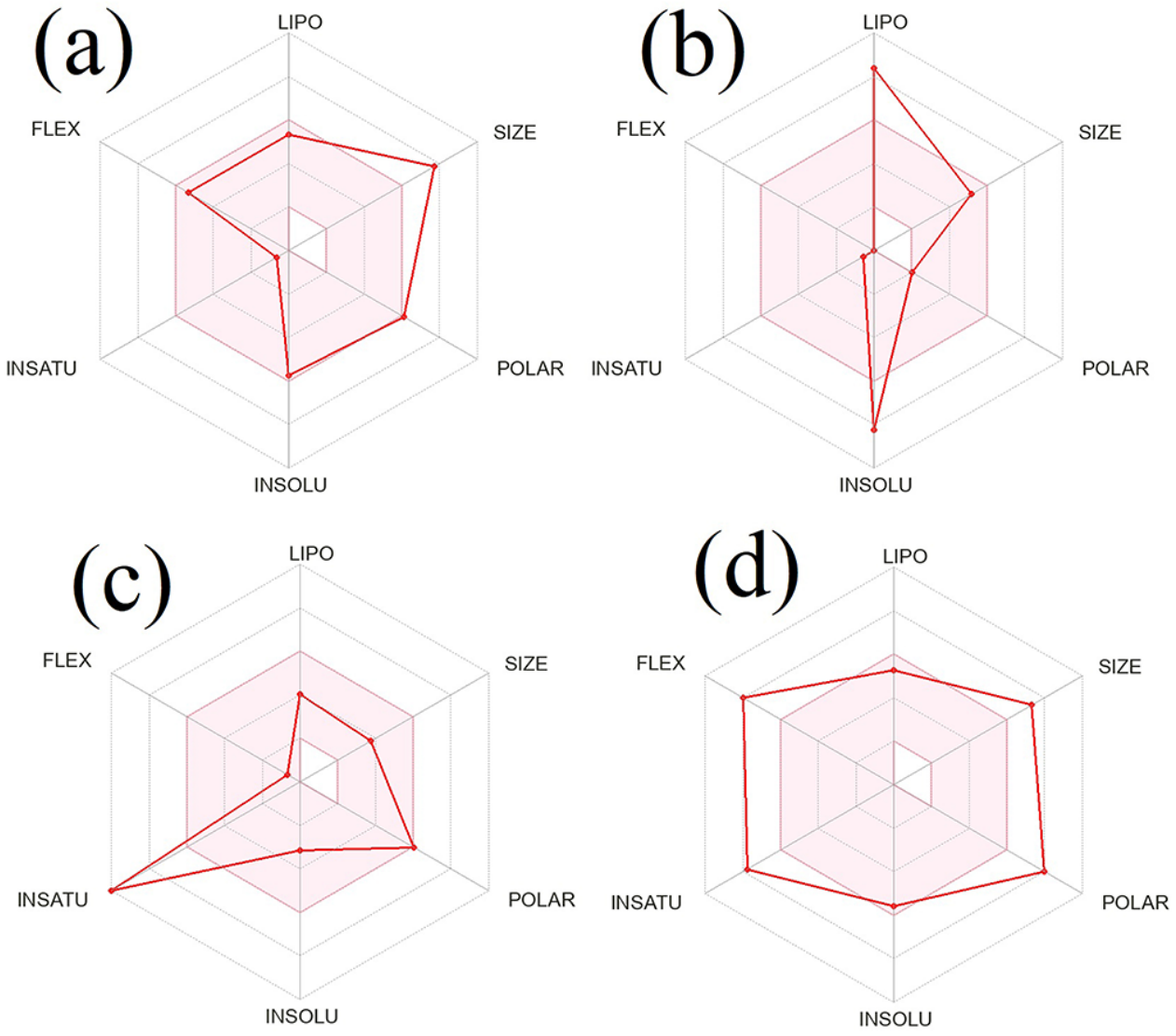

Figure 5

Bioavailability radar plot for oral bioavailability of top scored phytocompounds. Hemidescine (a), Beta-Amyrin (b), Quercetin (c), and standard drug (CPUY192018) (d). The pink area exhibits the optimal range for each property (Lipophilicity as XLOGP3 between −0.7 and +5.0; Size as molecular weight between 150 and 500 g mol−1; Polarity as TPSA (topological polar surface area) between 20 and 130 Å2; Insolubility in water by log S scale not higher than 6; Insaturation as per fraction of carbons in the sp3 hybridization not less than 0.25 and Flexibility as per rotatable bonds no more than 9).

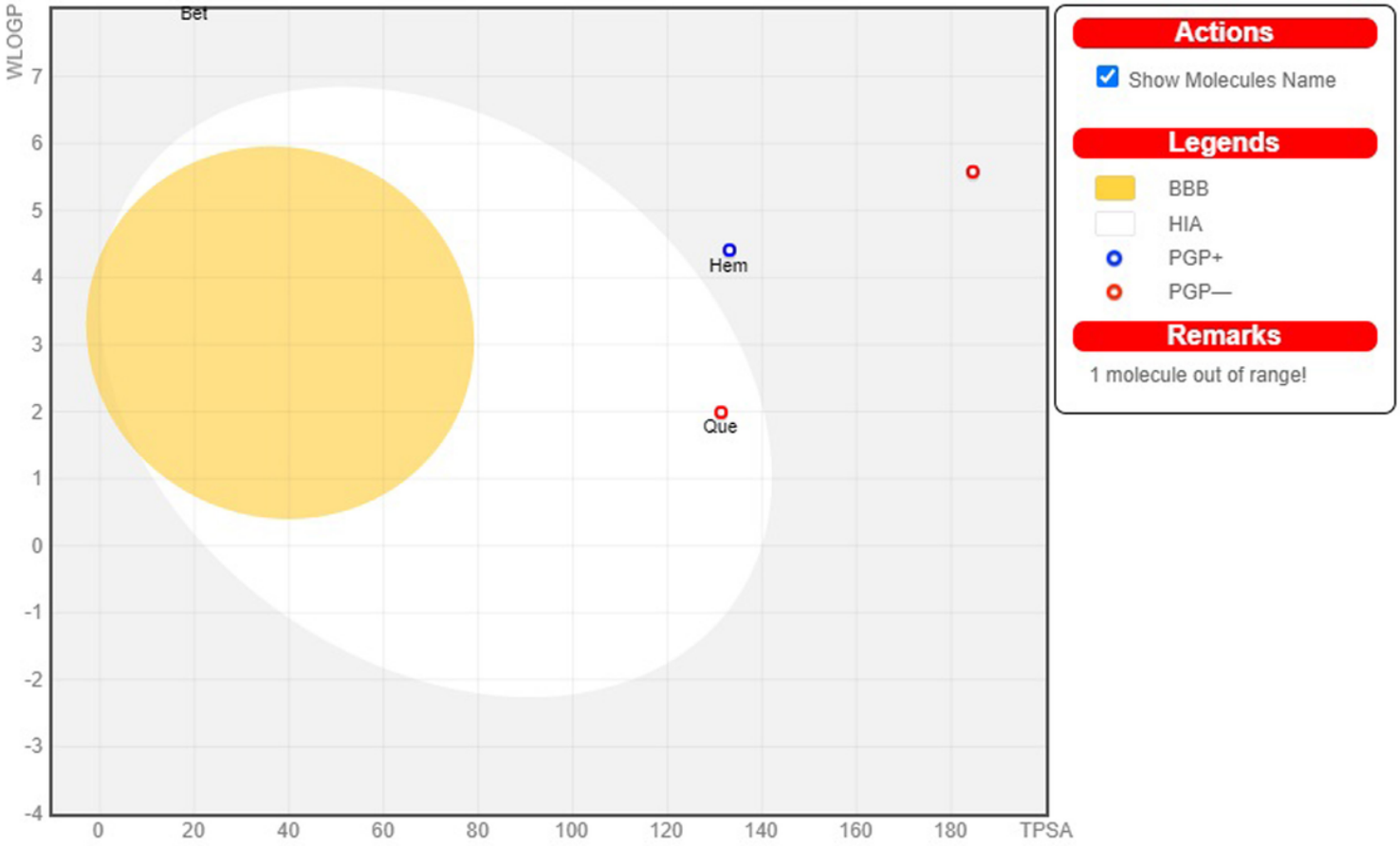

Figure 6

The EGG-BOILED model for the top scored phytocompounds and standard drug CPUY192018. The EGG-BOILED represents for intuitive evaluation of passive gastrointestinal absorption (HIA) white part and brain penetration (BBB) yellow part as well as substrates (PGP+) and non-substrates (PGP–) of the permeability glycoprotein (PGP) are represented by blue and red colour circles, respectively, of the selected bioactive compound and standard MAPK6 inhibitor in the WLOGP-versus-TPSA graph. The grey region is the physicochemical space of compounds predicted to exhibit high intestinal absorption.

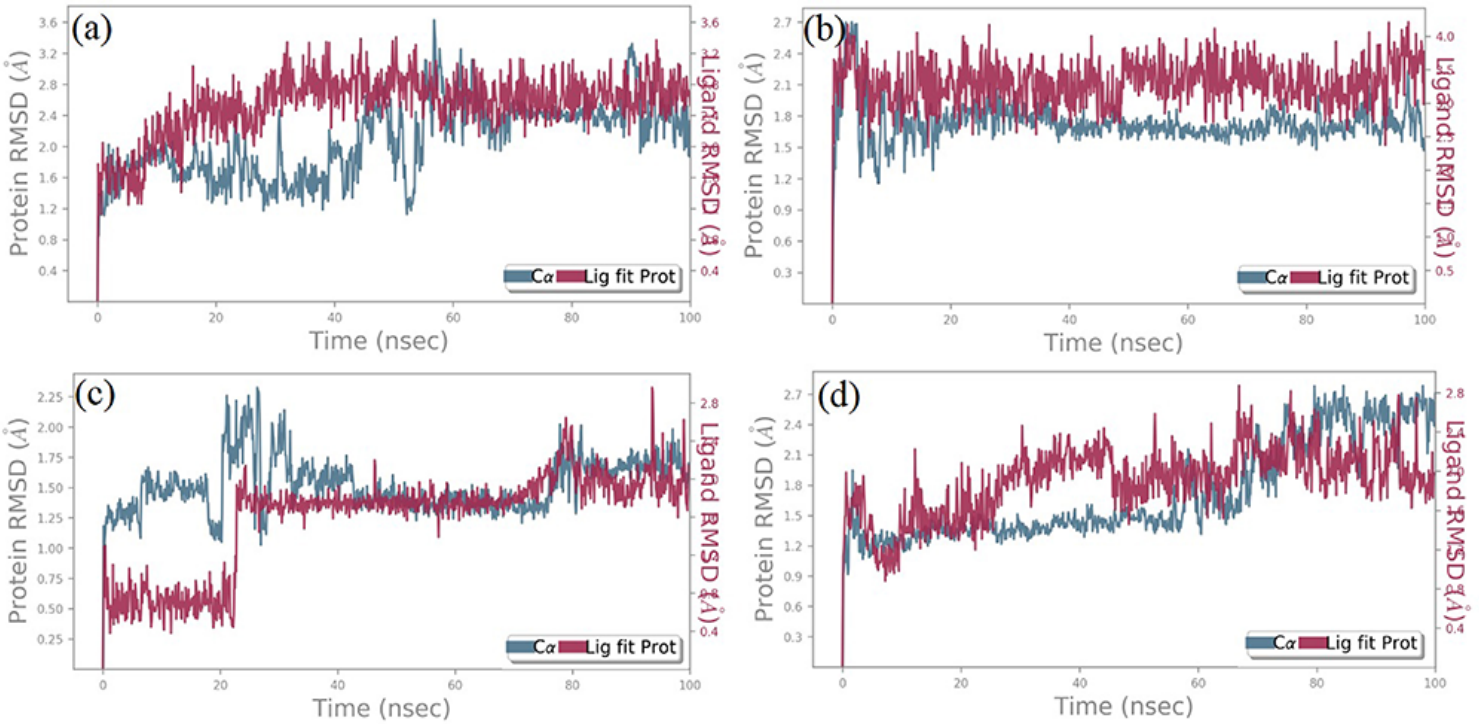

Figure 7

RMSD study plot for 100 ns MD Simulation of Hemidescine-Keap1 protein docked complex(a), Beta-Amyrin-Keap1 protein docked complex (b), Quercetin-Keap1 protein docked complex (c), and standard drug CPUY192018-Keap1 protein docked complex (d).

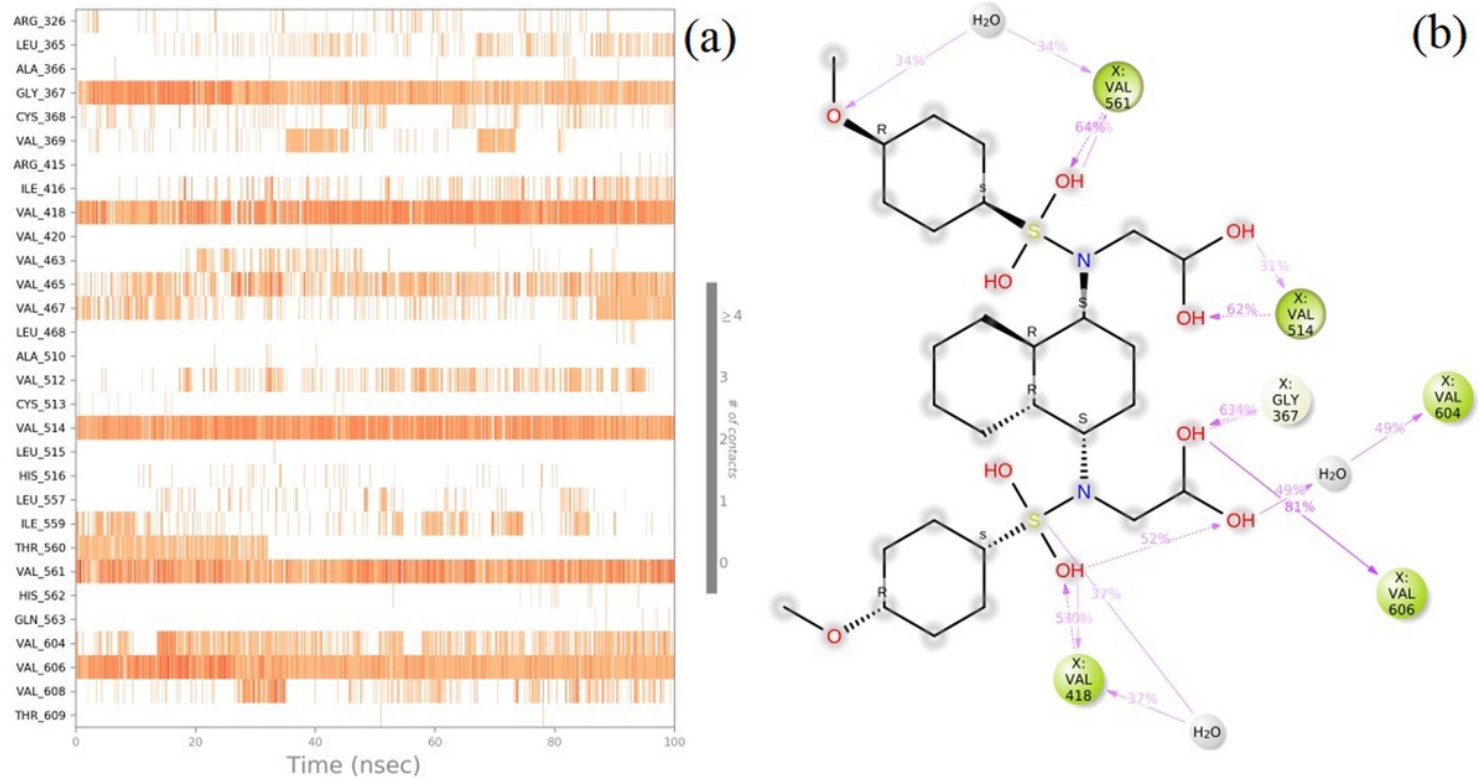

Figure 8

Hemidescine-Keap1 protein contacts timeline representation (a); and Hemidescine contacts with respective to the amino acids in the target protein Keap1 (b).

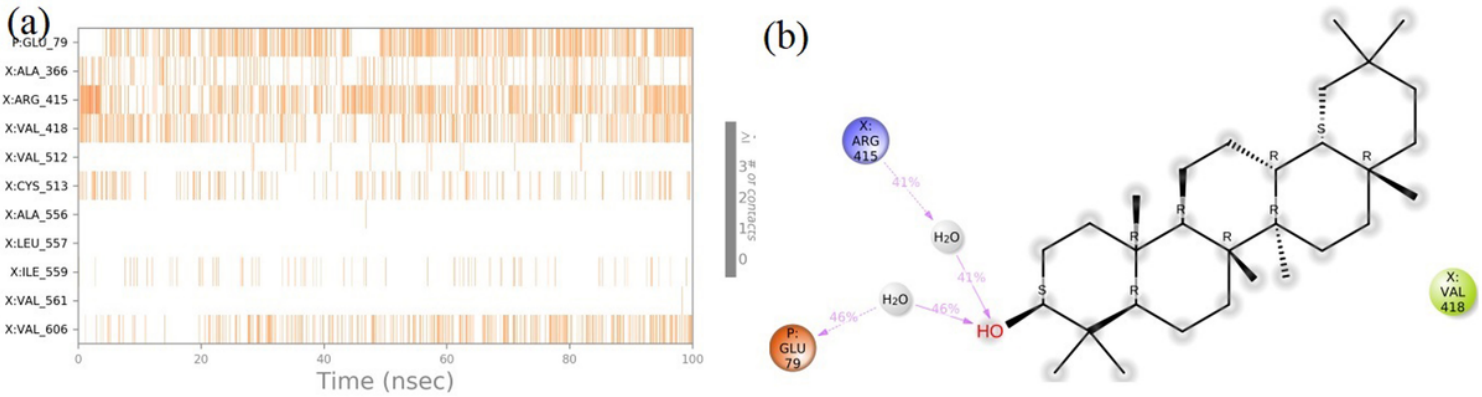

Figure 9

Beta-Amyrin-Keap1 protein contacts timeline representation (a); and Beta-Amyrin contacts with respective to the amino acids in the target protein Keap1 (b).

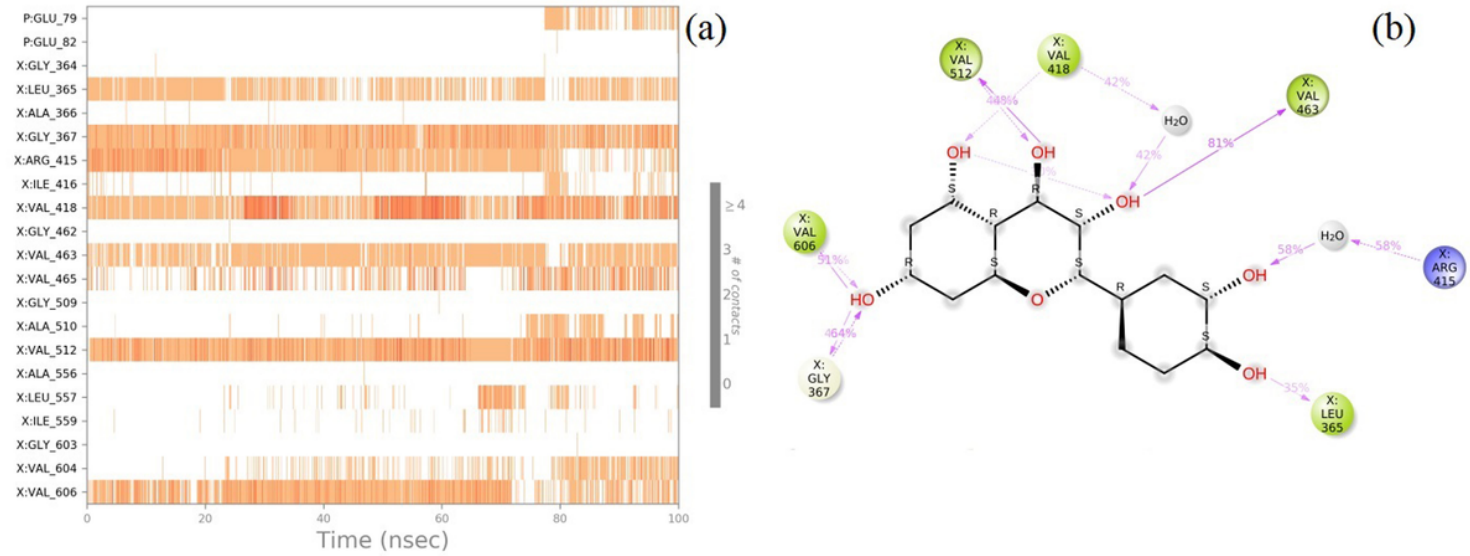

Figure 10

Quercetin-Keap1 protein contacts timeline representation (a); and Quercetin contacts with respective to the amino acids in the target protein Keap1 (b).

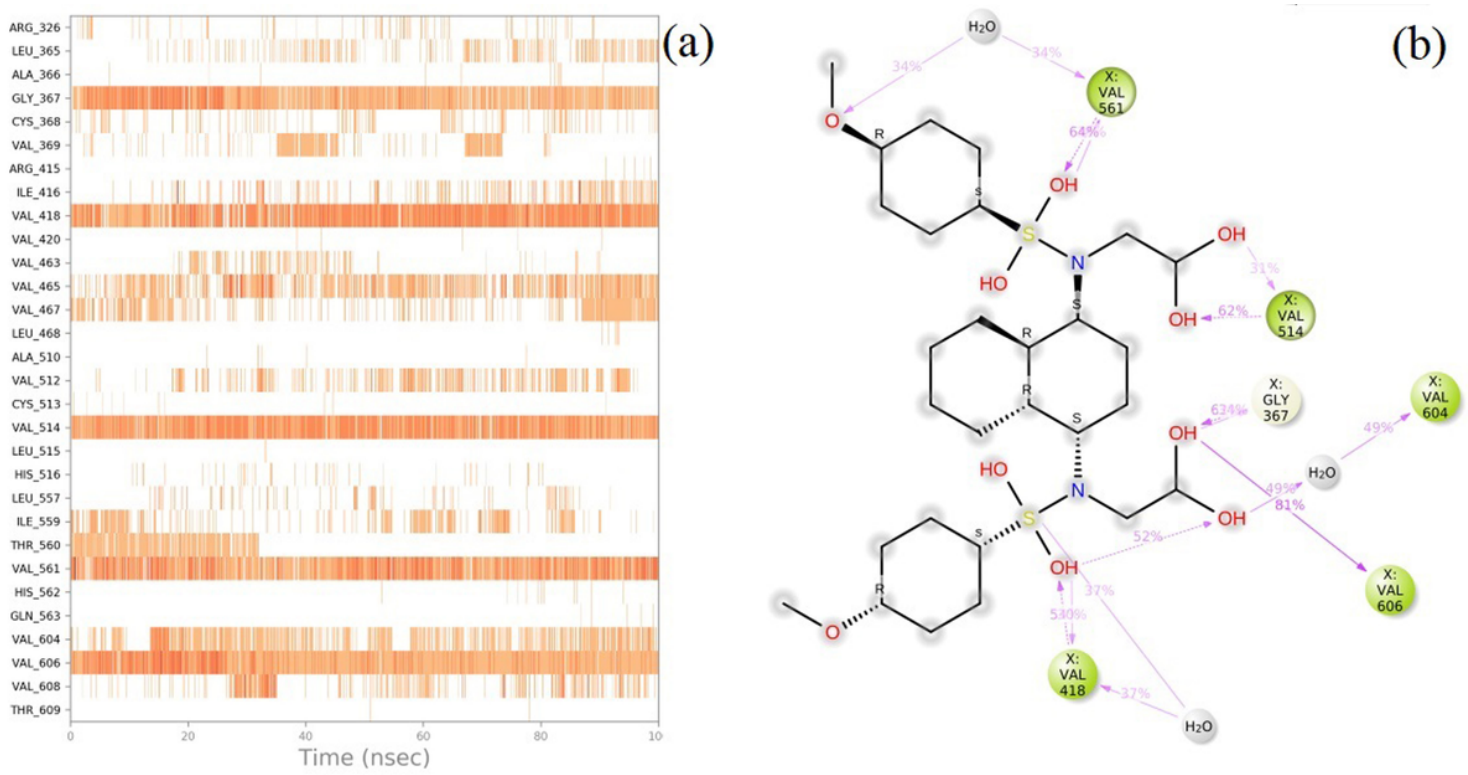

Figure 11

CPUY192018-Keap1 protein contacts timeline representation (a); and CPUY192018 contacts with respective to the amino acids in the target protein Keap1 (b).

Image not available with this version

Figure 12

RMSF of the Hemidescine for characterizing changes in the ligand atom positions (a), RMSF of the Beta-Amyrin for characterizing changes in the ligand atom positions (b), RMSF of the Quercetin for characterizing changes in the ligand atom positions (c), and RMSF of the CPUY192018 (standard drug) for characterizing changes in the ligand atom positions.

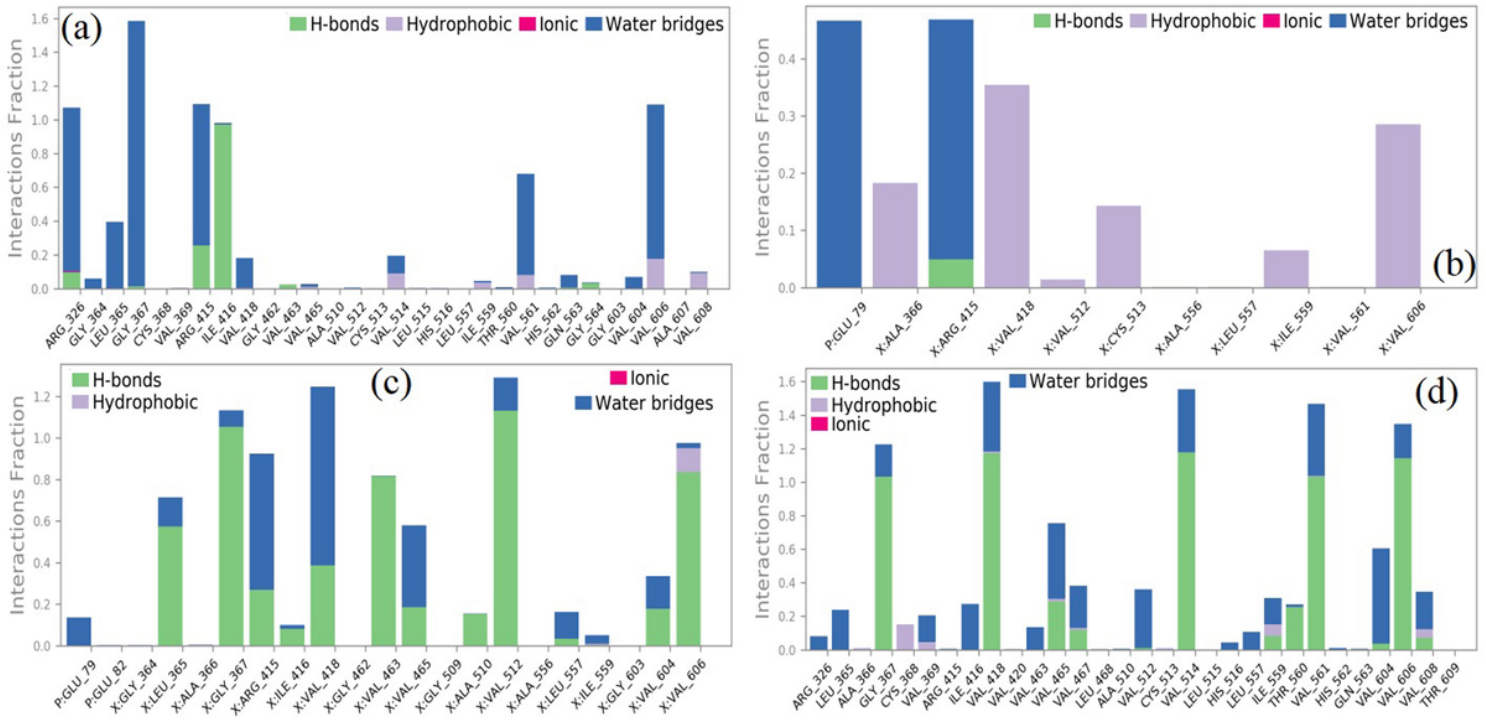

Figure 13

Percentage of amino acid and water mediated interactions contribution in MD simulations with Hemidescine (a), Beta-Amyrin (b), Quercetin (c), and standard drug (CPUY192018) (d).